ON THE PARAMETRIC EXCITATION OF A TENSIONED SHEET WITH AN EDGE CRACK

A THESIS

Presented to

The Faculty of the Division of Graduate

Studies and Research

By

Som P. S. Virk

In Partial Fulfillment

of the Requirements for the Degree

Doctor of Philosophy

in the School of Aerospace Engineering

Georgia Institute of Technology

September, 1975

ON THE PARAMETRIC EXCITATION OF A TENSIONED SHEET WITH AN EDGE CRACK

Approved:

Robert L. Carlson, Chairman

Stanley C. Bailey

G. Alvin Pierce

Date approved by Chairman: June 4, 1975

ACKNOWLEDGMENTS

I would like to express my profound gratitude to my dissertation advisor, Dr. Robert L. Carlson, for his fine ideas, valuable advice, useful discussions and encouragement during the course of this research work.

I would like to extend grateful appreciation to Dr. G. A. Pierce for his reading and valuable suggestions of the manuscript. I would also like to thank the other members of my reading committee, Dr. J. M. Anderson, Dr. L. Z. Emkin and Dr. S. C. Bailey for their help and constructive criticism during the course of this work.

Acknowledgments are also due to the School of Aerospace Engineering for the award of a research assistantship.

Finally, I am grateful to my parents and my friend Becky Braswell for their love and encouragement.

TABLE OF CONTENTS

TABLE OF CONTENTS (Continued)

LIST OF TABLES

LIST OF ILLUSTRATIONS

NOMENCLATURE

P_o	static mean load
P_1	amplitude of time dependent load
λ	frequency of time dependent load
ω	free transverse vibration frequency
w	transverse deflection
t	time
E	modulus of elasticity
I	area moment of inertia
m_1	mass per unit length of rod
m	mass per unit area of plate
λ_1	eigenvalue corresponding to tensile buckling problem
h	plate thickness
q(x,y)	transverse loading per unit area of plate
D	flexural rigidity of the plate
∇^2	Laplacian operator
x	rectangular coordinate of a point in plane of plate
y	rectangular coordinate of a point in plane of plate
z	rectangular coordinate of a point in transverse direction of plane
ψ	Airy stress function
w_o	initial imperfections of plate in transverse direction
N_x	tensile force in x-direction per unit length of plate
N_y	tensile force in y-direction per unit length of plate

N_{xy}	shear force per unit length of plate
$f_k(t)$	unknown functions of time
ℓ_1	length of the simply supported rod
$\phi_k(x,y)$	admissible functions in space x and y
ℓ	half the plate length
ν	Poisson's ratio
M_x	bending moment per unit length about y-axis
M_y	bending moment per unit length about x-axis
V_x	shear resultant on face of plate parallel to y-axis
V_y	shear resultant on face of plate parallel to x-axis.
L	Lagrangean
T	kinetic energy of a system
π	total potential energy of a system
U	internal potential of a system
V	external potential of a system
ρ	density of plate material
g	acceleration due to gravity
$\bar{w}(x,y,t)$	transverse deflection of plate, function of x,y, and t
σ_x	normal stress in x direction
σ_y	normal tensile stress in y-direction
σ_{xy}	shear stress in x direction on face of plate whose outward drawn normal is directed in y-direction
σ_{xt}	normal stress in x direction due to alternating inplane load
σ_{yt}	normal stress in y direction due to alternating inplane load.
σ_{xyt}	shear stress due to alternating inplane load.
$\alpha_{k\ell}$	matrix elements for kinetic energy

$\beta_{k\ell}$ matrix elements for internal potential

$\gamma_{k\ell}$ matrix elements for external potential

c inplane mean force parameter

d inplane alternating force parameter

$\underline{\alpha}$ kinetic energy square matrix

$\underline{\beta}$ internal potential square matrix

$\underline{\Gamma}$ external potential square matrix

$\underset{\sim}{f}$ column matrix of time dependent function

a crack length

b width of the plate

r polar coordinate

θ polar coordinate

θ_x rotation about x axis

θ_y rotation about y axis

c_1, c_2, c_3 unknown functions of time in symmetric trigonometric function

c_4, c_5 unknown functions of time in antisymmetric trigonometric function

c_6, c_6, c_8 unknown functions of time in symmetric polynomial function

c_9, c_{10} unknown functions of time in antisymmetric polynomial function

{F} nodal forces column matrix due to distributed loads

{R} externally applied nodal force column matrix

[K] square stiffness matrix

$\{\delta\}$ nodal displacement column matrix

$\alpha_1, \ldots, \alpha_{12}$ unknown coefficients of displacement function

A_i area of i^{th} element

$w_k^{(i)}$ k^{th} mode displacement of i^{th} element

$w_\ell^{(i)}$ ℓ^{th} mode displacement of i^{th} element

N	total number of elements
G	modulus of rigidity

SUMMARY

The objective of this dissertation is to describe results of an experimental and analytical investigation of the parametric excitation of a tensioned sheet with an edge crack. The free vibration and static tensile buckling are studied as special cases. The effect of crack length on the free vibration, static tensile buckling and dynamic behavior is emphasized.

The homogenous, linear governing differential matrix equations for the dynamic stability problem are obtained by using assumed modes in Lagrange's Equations. The special cases of free vibration and tensile buckling are obtained by setting certain quantities to zero.

The free vibration analytical results obtained by the use of a finite element method (STRUDL - Structural Design Language) correlate well with the experimental results. The finite element method is also used for the analysis of the initial nonuniform stress state.

The correlation between dynamic stability experimental results and analytical results obtained by using a fundamental free vibration mode is good enough to be useful in predicting the dynamic stability behavior.

The free vibration frequencies decrease by about 20 percent as the crack length to plate width ratio increases from zero to 0.8. The overall effect of increasing this ratio on dynamic stability is to increase the size of the unstable zones and to cause them to occur at lower frequencies.

CHAPTER I

INTRODUCTION

Concept of Static and Dynamic Stability

A survey of the type and form of structural elements developed over the past two hundred years reveals a continuing trend towards light, thin and high strength structures. The most obvious examples of the use of light and thin structures to achieve economic service life are to be found in aerospace structures. Also the use of lighter and high strength components in bridge construction enables longer unsupported spans to be employed. In addition, reductions in the cost of supporting systems are achieved.

In the use of low strength materials, bodies designed to meet the strength requirements must be so stout that failure due to instability is not often a problem. It is when both strength and low weight are required that the problem of stability becomes a design factor.

Consider a problem in which a number of static forces (forces that are not a function of time) act on the system, and the load, P, is the parameter representing them. Then as the load is increased, a classification of the response developed may be based on a consideration of the displacements of the system. Consider an n-degree of freedom system in which the displacements,

$$\bar{q}_k - \bar{q}_k^{(o)} = a_k \quad (k = 1,2,3,\ldots,n)$$

represent the equilibrium configuration of the loaded system measured from some initial configuration state $\bar{q}_k^{(o)}$. If an unacceptable value of at least one a_k occurs, the system may have developed an unstable configuration. The level of unacceptable values depends upon the system and its allowable stresses. Problem of this type are called static stability problems due to the static nature of the loading.

In some cases the loading applied can either be a function of time or it can be a combination of static loads and time-dependent loads. The consequences of the differences in the type of loading can be illustrated by a simple example. Consider a straight rod which is subjected to a static load P_o. When the load is negative (compressive), and it is increased, a value is achieved for which the rod will become statically unstable. This load, designated as P_{cr}, is called the buckling load. Now, assume that the static load P_o is replaced by the time-dependent load $P_1 \cos \lambda t$, where P_1 is the time-independent amplitude, λ is the frequency of excitation and t is the variable time. If the amplitude of the load, P_1, is less than the static buckling load. P_{cr}, then the rod may experience only longitudinal vibrations. It can, however, be shown that for certain relationships between the disturbing frequency, λ, and natural frequency of transverse vibrations, ω, a straight rod becomes dynamically unstable, and transverse vibrations can occur [5].

If the rod is subjected to a combination of static and time-dependent loading of the type $P_o + P_1 \cos \lambda t$ (see Figure 1), the nature of the dynamic response depends on the values of P_o, P_1 and λ. A stability plot can, in fact, be made in parameter space (P_o, P_1 and λ space) by studying

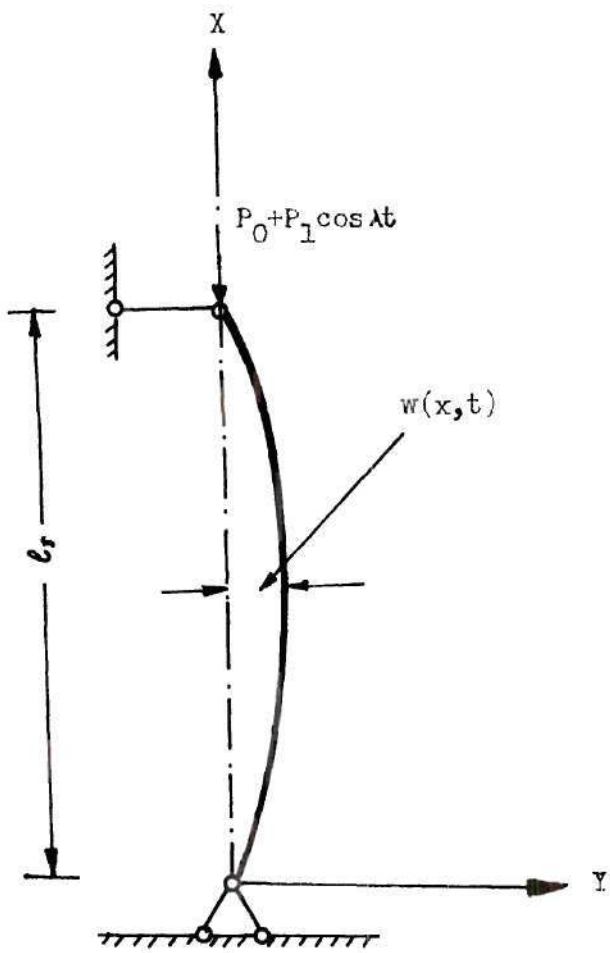

Figure 1. Rod Subjected to Static and Time Dependent Loading.

the motion of the rod for particular combinations of the loading parameters.

Historical Background of Dynamic Stability

N. M. Beliaev performed the first mathematical analysis of the dynamic stability of a hinged column in 1924 [1]. He considered the case of a column subjected to a force $P(t) = P_0 + P_1 \cos \lambda t$. For P_0 equal to a constant, he represented the instability regions in the λ - P_1 plane. In 1936, R. Einaudi solved the problem of a thin elastic plate subjected to in-plane loading [2]. Among the other notable investigators of dynamic stability of plates were Chelomei [3] and Bodner [4]. More recently, Bolotin [5] developed solutions for problems of both linear and non-linear dynamic stability in plates. In 1965, Somerset and Evan-Iwanowski [6] studied the effect of in-plane inertia forces, and in 1969, Willems and Duffield [7] investigated the effect of closely spaced stiffeners on the dynamic stability of plates.

Recently, some investigations have been conducted on the free-vibration and the dynamic stability of plates with cut outs and internal as well as edge cracks. Stahl and Keer [8] studied the vibration of cracked rectangular plates with all sides simply supported. They used the Levy-Nadai approach, and the Hankel transform was used to satisfy the stress free boundary conditions at the crack surface. Their results included a stress singularity of the correct order at the crack tip. Lynn and Kumbasar [9] used a similar approach, but made no attempt to incorporate a stress singularity at the crack tip. This method of solution for other boundary conditions (e.g., a combination of free and fixed)

would be difficult and perhaps not possible.

Some additional work on cracked plates has been performed by Knowles and Wang [10], and Hartranft and Sih [11]. Lukaart [12] investigated the use of the assumed modes method to determine the free vibration frequencies for a plate with an edge crack. His results do not, however, correlate well with available experimental data.

Recently Petyt [13] analyzed the vibration characteristics of a tensioned plate containing a fatigue crack. He used a finite element displacement approach. He calculated the variation of buckling stress and frequency of fundamental mode with crack length and different levels of applied tensile force. Backer [14] and Datta [15] studied both, the static and cynamic behavior of tensioned doubly connected plates. In 1973, Carlson [16] conducted an experimental study of the parametric excitation of a tensioned sheet with a cracklike opening. His specimen consisted of a sheet of plexiglass with two opposite sides supported and the other two sides free. The opening was in the center of the sheet, parallel to the supported sides. These results appear to provide the only data available on dynamic stability problems in which the initial stress state is of the type developed in cracked elements.

Features of the Parametric Excitation Problem

Whenever static loading of a particular kind causes a loss of static stability (see Figure 1), vibrational loading of the same kind can cause a loss of dynamic stability. For a rod, such loading is characterized by the fact that it is contained as a parameter on the left hand side of the governing Equation of motion as follows:

$$EI \frac{\partial^4 w}{\partial x^4} + (P_o + P_1 \cos \lambda t)\frac{\partial^2 w}{\partial x^2} + m_1 \frac{\partial^2 w}{\partial t^2} = 0 \qquad (1)$$

where,

w, is transverse deflection,

P_o, is a compressive load

P_1, λ and t are as described before,

E, is modulus of Elasticity,

I, is area moment of inertia, and

m_1, is mass per unit length of rod.

This type of loading is described as a parametric loading. To be more specific, the loadings are parametric with respect to only certain forms of deformations. As Equation (1) indicates, the above-mentioned longitudinal force compressing the straight rod is a parametric loading with respect to the transverse deflections but not with respect to the longitudinal deformations.

If the inertia term and the term containing the effect of time-dependent loading is eliminated, Equation (1) reduces to:

$$EI \frac{d^4 w}{dx^4} + P_o \frac{d^2 w}{dx^2} = 0 \qquad (2)$$

which is the well-known equation for static bending of a column as shown in Figure 1.

Similarly, if all the externally applied loadings (i.e., the static as well as the time-dependent loading) are neglected, Equation (1) reduces to:

$$EI \frac{\partial^4 w}{\partial x^4} + m_1 \frac{\partial^2 w}{\partial t^2} = 0 \qquad (3)$$

which represents the problem of free transverse vibration of a straight rod.

Considering the simple harmonic motion and separating the time and space variables, Equation (3) becomes the equation of motion involving the free vibration frequency ω as follows

$$EI \frac{d^4 w_1}{dx^4} - m_1 \omega^2 w_1 = 0 \qquad (3A)$$

where $w(x,t) = w_1(x)e^{i\omega t}$

and $w_1(x)$, is a function of x alone.

The above discussion leads to the conclusion that the problems of static bending and free vibration of structural elements in general are special cases of the dynamic stability problem involving parametric excitation.

Problems of Interest for Cracked Structural Elements

a. Non Uniform Stress State

When a uniform structural element is subjected to a constant loading, the stress state developed can be simple. If the structural element has holes or notches, the stress state developed becomes nonuniform. The stresses at some point or points may then be more than the nominal stress by a factor which is called the stress concentration factor. The structural discontinuity referred to may include internal flaws, openings, scratches and cracks, etc. In the case of a cracked structure the stresses near the crack tip may mathematically increase without bound; i.e., there

is a singularity at the crack tip. For example, consider a thin plate with an edge crack as shown in Figure 2. When a tensile load is applied, there will be a tensile stress concentration at the crack tip. Also, if the crack is sufficiently long, compressive stresses can be developed in a region of the type which has been shaded. These compressive stresses are the result of the bending moment developed by the pressure of the crack as shown in Figure 3.

b. Positive and Negative Eigenvalues for Buckling Problem

Returning to the problem of a straight rod, the governing differential equation for bending was Equation (2). Integrating Equation (2) twice with respect to x, and using hinged end boundary conditions to evaluate the constants of integration, the result can be written as:

$$\frac{d^2w}{dx^2} + \lambda_1 w = 0 \tag{4}$$

where $\lambda_1 = \frac{P_o}{EI}$

This is an eigenvalue problem and furnishes the positive eigenvalues, λ_1's. But if the compressive load, P_o, is replaced by a tensile load, Equation (4) becomes:

$$\frac{d^2w}{dx^2} - \lambda_1 w = 0 \tag{5}$$

This is not an eigenvalue problem; i.e., there is no buckling load. Thus for buckling to occur, the structure as a whole or at least some portions of it should be in compression. The thin plate with a crack shown in Figure 2 will buckle when subjected to a compressive load to

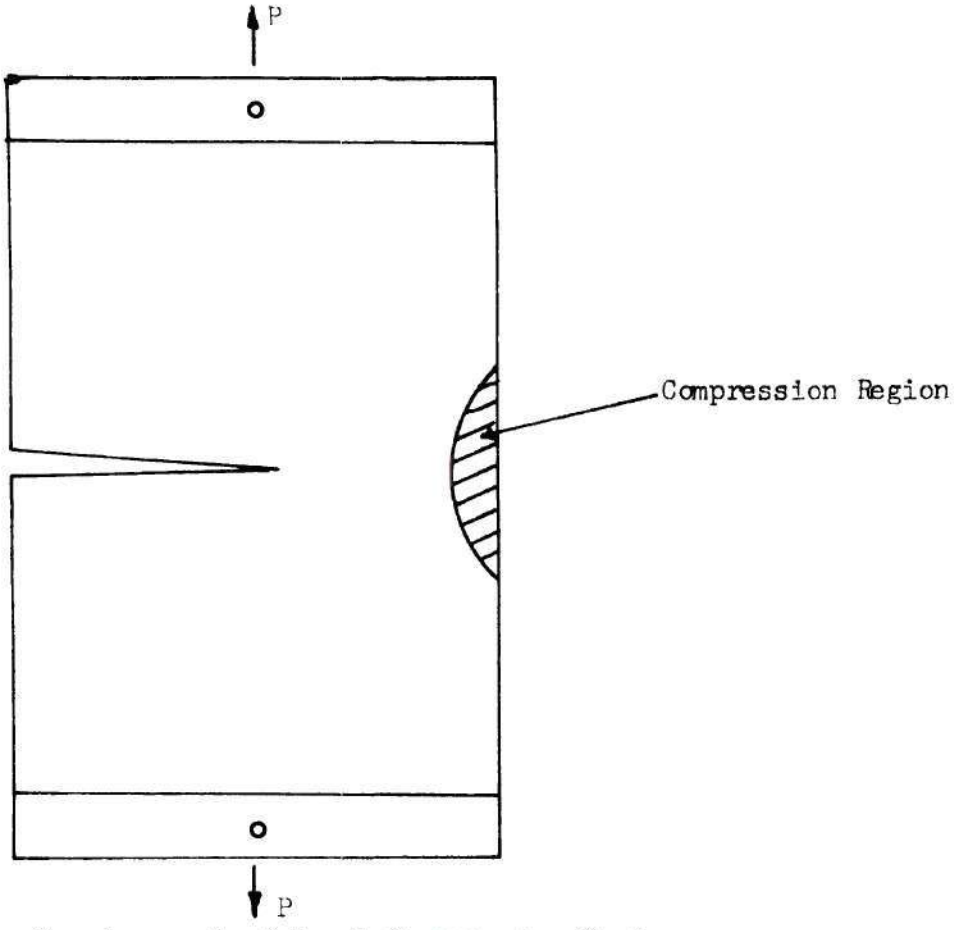

Figure 2. Developement of Local Compressive Region.

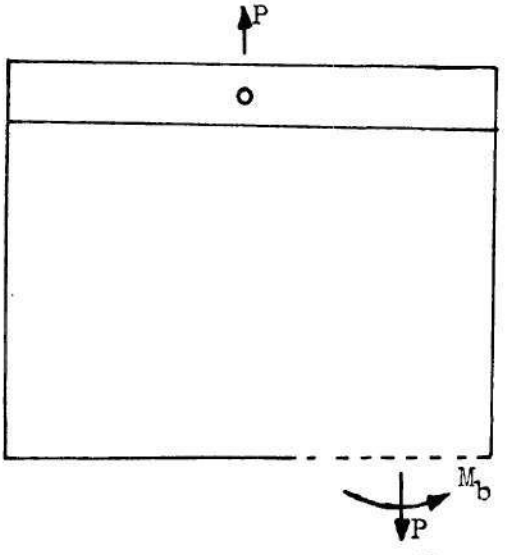

Figure 3. Local Tensile Buckling Phenomonon.

give positive eigenvalues just as in the case of a straight rod. But the significant feature of the thin plate with the edge crack is that it can also buckle when subjected to a tensile loading. The reason being the compressive areas developed as shown in Figure 3. For compressive loading, the out-of-plane deflection accompanying buckling is global in character. For tensile loading, however, buckling occurs with a more localized out-of-plane deflection.

c. Stabilizing Effect of Tension Versus Compression

As discussed before, static stability is a special case of dynamic stability, and both are sensitive to the typical external loadings in the same sense. A straight rod buckles statically only under a compressive load. Dynamic instability can, however, be developed under either compressive or tensile mean loads. Under compressive load, however, the regions of instability are larger; i.e., the tension has a stabilizing influence.

In the case of the thin sheet with an edge crack, the static buckling can occur both under tensile loading and compressive loading. Clearly, a mean compressive loading would be expected to have a destabilizing influence. The effect of mean tensile load remains an open question, however.

Objective of Current Research

The objective of the investigation described in this dissertation is to conduct an experimental and analytical investigation of the static and dynamic stability of a tensioned sheet with an edge crack. In the dynamic case, the sheet is subjected to a parametric excitation. Two

opposite sides of sheet are free and the other two sides which are parallel to the edge crack are clamped. A diagrammatic sketch is shown in Figure 4. All the special features discussed in the preceding section exist in this special problem. Namely, the stress state is non-uniform, and there are positive as well as negative eigenvalues for the static buckling. The question of the mean tensile load being stabilizing or destabilizing is still open. Also, the nature of the response developed can be expected to have an influence on crack growth.

In the investigation described here, the sheet was subjected to both a constant mean load and a cyclic load. The boundaries defining transition from stable to unstable dynamic stability regions were determined in terms of the mean load, cyclic load and the excitation frequency. The effect of crack length on the size of the instability regions was also studied. In addition, the free vibration and static buckling problems were considered as special cases of the parametric excitation problem.

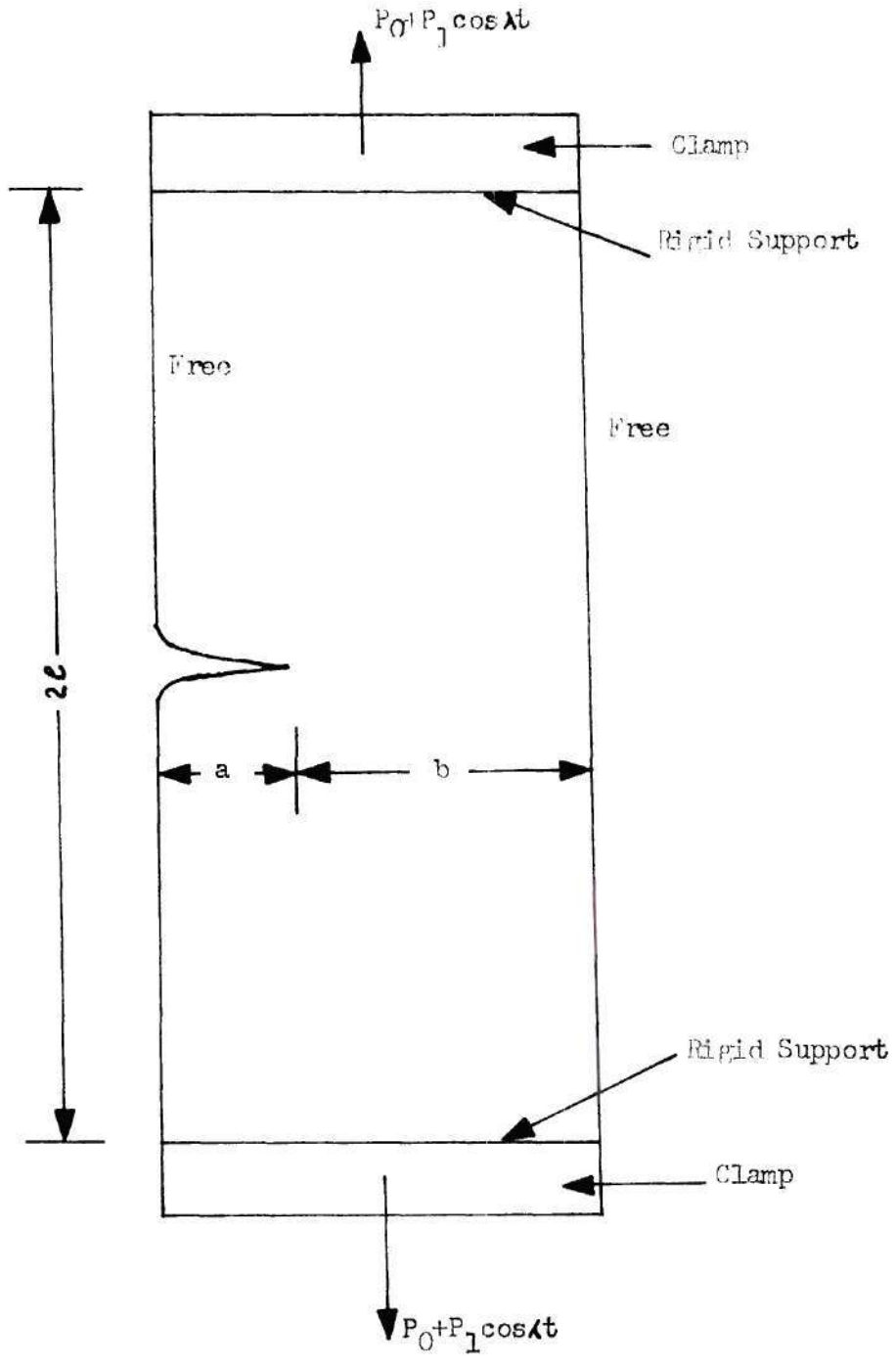

Figure 4. Model for Parametric Excitation Problem.

CHAPTER II

THEORETICAL CONSIDERATIONS

Governing Equations

The bending theory of thin, initially flat plates made of linearly elastic, isotropic and homogenous material is based on the assumption that straight lines initially normal to the middle surface remain straight and normal to that surface after deformation [17]. When the lateral deflections are much less than the thickness of the plate ($w << h$), the theory is called the small deflection theory, which has been available for over one hundred years. According to this theory, the deformation is governed by the equation

$$\nabla^4 w = \frac{q(x,y)}{D} \tag{6}$$

where ∇^2 is the two dimensional Laplacian operator, and $\nabla^2 \cdot \nabla^2 = \nabla^4$. Thus,

$$\nabla^4 w = \frac{\partial^4 w}{\partial x^4} + 2\,\frac{\partial^4 w}{\partial x^2 \partial y^2} + \frac{\partial^4 w}{\partial y^4}\ ,$$

q is the transverse load per unit area, which may be a function of location.

D is the flexural rigidity of the plate.

As deflections become moderately large, membrane forces due to bending of the plate can influence the deformed shape. In fact, only

if the deformed state is a developable surface will middle surface stretching be absent. Often, however, a plate is prevented by constraints from deforming into such a surface and increasing deflections lead to increasing membrane forces which are functions of position. The effect of stretching is incorporated in equations which were derived by Merguerre [18]. In cartesian coordinates, x and y, these equations are

$$\nabla^4\psi = Eh\left[\left(\frac{\partial^2 w}{\partial x\partial y}\right)^2 - \left(\frac{\partial^2 w_o}{\partial x\partial y}\right)^2 - \left(\frac{\partial^2 w}{\partial x^2}\cdot\frac{\partial^2 w}{\partial y^2} - \frac{\partial^2 w_o}{\partial x^2}\cdot\frac{\partial^2 w_o}{\partial y^2}\right)\right] \tag{7}$$

$$D\nabla^4(w - w_o) = \frac{\partial^2\psi}{\partial x^2}\cdot\frac{\partial^2 w}{\partial y^2} + \frac{\partial^2\psi}{\partial y^2}\cdot\frac{\partial^2 w}{\partial x^2} - 2\frac{\partial^2\psi}{\partial x\partial y}\cdot\frac{\partial^2 w}{\partial x\partial y} + q(x,y) \tag{8}$$

where ψ is the Airy stress function such that the membrane forces per unit length are

$$N_x = \frac{\partial^2\psi}{\partial y^2}\ ,\ N_y = \frac{\partial^2\psi}{\partial x^2}\ ,\ N_{xy} = \frac{\partial^2\psi}{\partial x\partial y} \tag{9}$$

and w_o is the initial imperfection function in the transverse direction. The function w, is the total deflection measured from the x-y plane.

These equations for $w_o = 0$, were obtained by Karman. An examination of these equations reveals that they are nonlinear and coupled in the transverse deflection, w, and the Airy stress function, ψ. If $w_o = 0$

is substituted into Equation (8), the right hand side of this equation gives the Gaussian curvature which is a measure of mid-surface stretching due to bending. A developable surface has a Gaussian curvature of zero. For the case of motion in the transverse direction of the plate, the transverse inertia force, $m \frac{\partial^2 w}{\partial t^2}$, can be identified as a part of the lateral loading. In this inertia term, m is the mass per unit area of the plate and t is time. The above two equations then are the equations of motion for the dynamic case.

Solutions of the non-linear, coupled differential equations are very difficult to obtain. If it is assumed that the Gaussian curvature is small so that the mid-surface stretching due to bending can be neglected, then equation (7) reduces to

$$\nabla^4 \psi = 0 \ . \tag{10}$$

which is subject to prescribed in-plane boundary conditions on ψ. The problem described is a plane stress problem and the solution of Equation (10) provides the stress distribution (N_x, N_y, N_{xy}) in the plate.

Once the solution to the plane stress problem is obtained, substitution of ψ in terms of forces per unit length, in Equation (8) gives,

$$D\nabla^4 w = q - m \frac{\partial^2 w}{\partial t^2} + N_x \frac{\partial^2 w}{\partial x^2} + N_y \frac{\partial^2 w}{\partial y^2} + 2N_{xy} \frac{\partial^2 w}{\partial x \partial y} \tag{11}$$

Here $w_o = 0$; i.e., the plate is assumed to be initially flat.

In many problems which have been solved the coefficients N_x, N_y and N_{xy} are either constants or in some cases only one is non-zero. In

a few instances problems in which these coefficients are functions of x and y have been considered.

Finally, problems in which these coefficients can be functions of time are also encountered. In the problem under investigation in this dissertation, these coefficients are functions of x and y and they are periodic in time, t; i.e., the structural elements of interest are subjected to parametric excitation.

Solution Procedures

In order to describe the solution alternatives available for analyzing the dynamic stability of a system which is excited parametrically first consider the case of the simply supported straight column shown in Figure 1. The governing differential equation for the problem is Equation (1). Separation of time and space variables can be achieved by use of solutions of the form

$$w(x,t) = f_k(t) \sin \frac{k\pi x}{\ell_1} \quad (k = 1,2,3,\ldots) \tag{12}$$

where $f_k(t)$ are unknown functions of time. Equation (12) satisfies the boundary conditions of the problem requiring that the deflection, together with its second derivative with respect to x, vanish at the ends of the column. By substituting Equation (12) into Equation (1), and using the separation of variables scheme, the space variable may be eliminated. The resulting equation which must be satisfied is an ordinary differential equation which is called the Mathieu equation. Considerations of the dynamic stability of the parametrically excited column thus require an analysis of the properties of the Mathieu equation.

If the same type of procedure is followed for the problem of dynamic stability of a cracked rectangular plate of Figure 5, a solution of the following form should be obtained.

$$w(x,y,t) = f_k(t)\ \phi_k(x,y) \tag{13}$$

Here again the $f_k(t)$'s are unknown functions of time. The functions, $\phi_k(x,y)$, which satisfy the boundary conditions of the problem should be sought. When these functions are substituted into the governing partial differential equation of the problem (Equation (11)), they should permit a separation of the space and time variables. A search for such functions quickly reveals that this is not possible for the cracked plate. It may, therefore, be concluded that the solution procedure which is effective for the column, cannot be used in the present investigation.

Since the independent variables of the governing differential equation involve both time and space, the direct use of approximation techniques for the boundary value problem are not suitable. Thus, the Galerkin and Raleigh-Ritz procedures [19] are eliminated. The Kantrovich method [19] might, however, appear to provide an acceptable basis for a solution procedure. This method may be viewed as a generalization of the Galerkin method in which solutions of the form of Equation (13) are again sought after acceptable functions for $\phi_k(x,y)$ are selected. Instead of obtaining a system of algebraic equations as in the Galerkin method, however, a system of ordinary differential equations in $f_k(t)$ are obtained. The crucial restriction on the use of this method is the

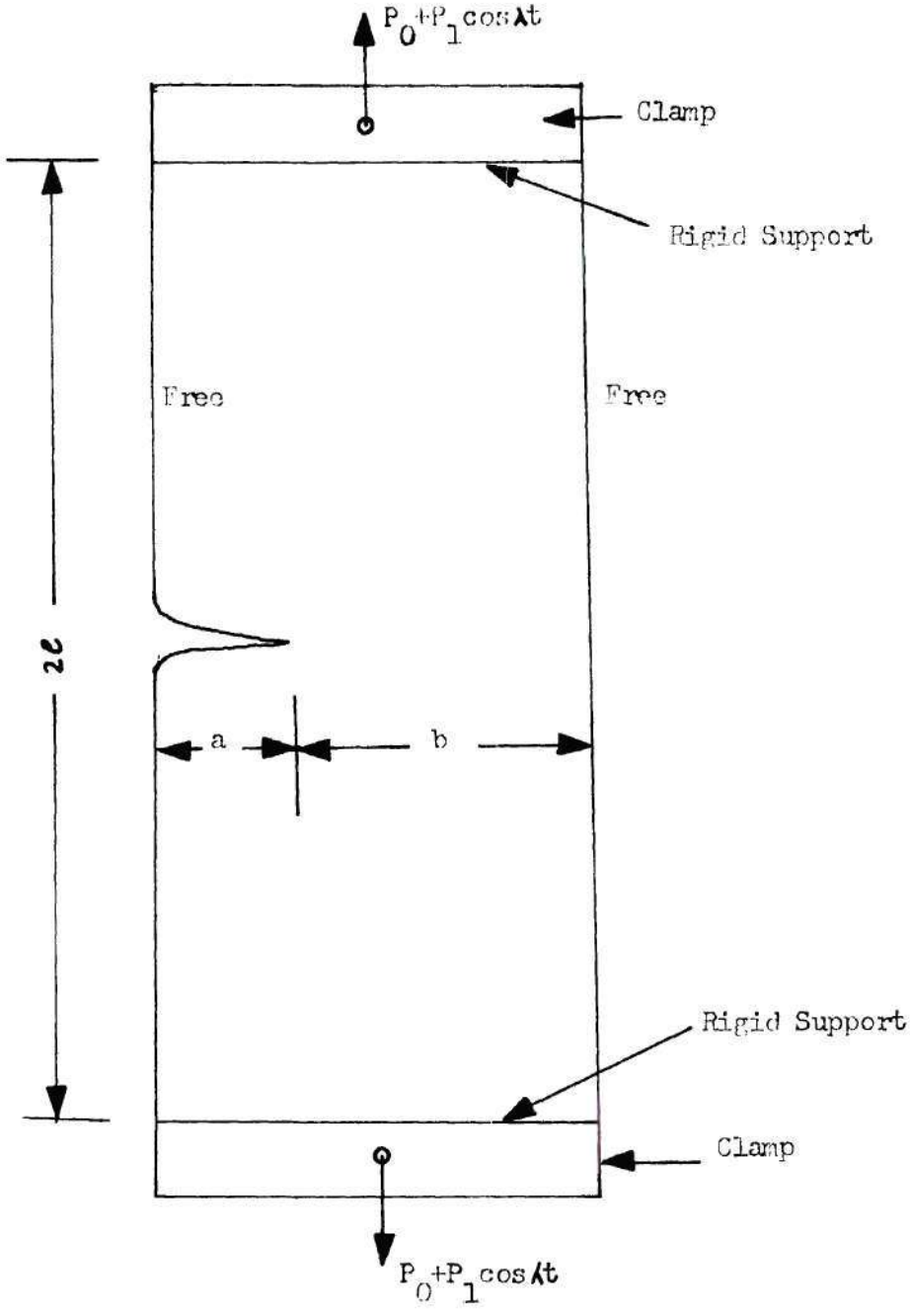

Figure 5. Model for Parametric Excitation Problem.

stipulation regarding the selection of "acceptable" functions, ϕ_k. These functions must satisfy all boundary conditions for the problem considered; i.e., both geometric and natural boundary conditions. For the cracked plate problem investigated here, the boundary conditions are (see Figure 5) as follows:

On $y = \pm \ell$

$$w = 0 \tag{14}$$

and

$$\frac{\partial w}{\partial y} = 0 \tag{15}$$

On $x = 0$ and $x = (a + b)$

$$M_x = -D\left(\frac{\partial^2 w}{\partial x^2} + \nu \frac{\partial^2 w}{\partial y^2}\right) = 0 \tag{16}$$

and

$$V_x = \frac{\partial^3 w}{\partial x^3} + (2 - \nu) \frac{\partial^3 w}{\partial x \partial y^2} = 0 \tag{17}$$

Finally on the crack faces; i.e., on $y = 0$, $0 \leq x < a$,

$$M_y = -D\left(\frac{\partial^2 w}{\partial y^2} + \nu \frac{\partial^2 w}{\partial x^2}\right) = 0 \tag{18}$$

and

$$V_y = \frac{\partial^3 w}{\partial y^3} + (2 - \nu) \frac{\partial^3 w}{\partial y \partial x^2} = 0 \tag{19}$$

In these equations, M_x and M_y are bending moments per unit length while V_x and V_y are the effective shear forces per unit length. Since it was not possible to find functions $\phi_k(x,y)$, which satisfy all of these boundary conditions, the use of the Kantrovich method was not considered further.

The solution procedure adopted for the present work is the assumed modes method [20] that makes use of Lagrange's equations. These equations may be written as

$$\frac{d}{dt}\left\{\frac{\partial L}{\partial \dot{f}_j}\right\} - \frac{\partial L}{\partial f_j} = 0 \qquad (20)$$

where $L = (T - \pi)$ is called Lagrangian.

T is Kinetic energy of the system

$\pi = (U - V)$ is the Potential energy of the system

U is the Internal Potential

and V is the External Potential.

The functions $f_k(t)$ are defined by the transverse deflection relation

$$\bar{w}(x,y,t) = \sum_{k=1}^{N} f_k(t) w_k(x,y) \qquad (21)$$

in which the $w_k(x,y)$ are N assumed modes which must satisfy the given geometric boundary conditions

The kinetic energy, $T = \frac{mh}{2} \int\int_{area} (\dot{\bar{w}})^2 dxdy$, where $m = \frac{\rho}{g}$, is the mass per unit volume of the plate.

ρ is the density of the plate material.

g is the Acceleration due to gravity

and h is the thickness of the plate.

Substituting for m in the kinetic energy expression,

$$T = \frac{\rho h}{2g} \int\int_{area} (\dot{\bar{w}})^2 dxdy \qquad (22)$$

The internal potential due to bending is defined as

$$U = \frac{D}{2} \int\int_{area} \left\{ \left(\frac{\partial^2 \bar{w}}{\partial x^2} + \frac{\partial^2 \bar{w}}{\partial y^2} \right)^2 - 2(1-\nu) \left[\frac{\partial^2 \bar{w}}{\partial x^2} \cdot \frac{\partial^2 w}{\partial y^2} - \left(\frac{\partial^2 \bar{w}}{\partial x \partial y} \right)^2 \right] \right\} dxdy \quad (23)$$

where $D = \frac{Eh^3}{12(1-\nu^2)}$ is the flexural rigidity of the plate.

The external potential may be transformed from boundary integrals to area integrals [17] and written as

$$V = -\frac{1}{2} \int\int_{area} \left[\bar{N}_x \left(\frac{\partial \bar{w}}{\partial x} \right)^2 + 2\bar{N}_{xy} \left(\frac{\partial \bar{w}}{\partial x} \cdot \frac{\partial \bar{w}}{\partial y} \right) + \bar{N}_y \left(\frac{\partial \bar{w}}{\partial y} \right)^2 \right] dxdy \quad (24)$$

where the coefficients $\bar{N}_x$, $\bar{N}_y$ and $\bar{N}_{xy}$ may be further defined as

$$\begin{aligned} \bar{N}_x(x,y,t) &= N_x + N_{xt} \cos \lambda t \\ \bar{N}_y(x,y,t) &= N_y + N_{yt} \cos \lambda t \\ \bar{N}_{xy}(x,y,t) &= N_{xy} + N_{xyt} \cos \lambda t \end{aligned} \quad (25)$$

These coefficients can also be expressed in terms of the in-plane stresses using

$$N_x = h\sigma_x, \quad N_y = h\sigma_y, \quad N_{xy} = h\sigma_{xy} \quad (26)$$

and

$$N_{xt} = h\sigma_{xt}, \quad N_{yt} = h\sigma_{yt}, \quad N_{xyt} = h\sigma_{xyt} \quad (27)$$

The stresses σ_x, σ_y, σ_{xy} are developed by the time-independent mean load, while σ_{xt}, σ_{yt}, σ_{xyt} are the stress amplitudes due to the

alternating in-plane load.

To determine U, V and T, partial derivatives of the transverse deflection function, $\bar{w}$, with respect to the time and space variables must be determined. Using summation convention (see Appendices A and B) the required expressions for T, U and V may be written as follows:

$$T = \alpha_{k\ell}\, \dot{f}_k\, \dot{f}_\ell \tag{28}$$

$$U = \beta_{k\ell}\, f_k\, f_\ell \tag{29}$$

$$V = -\gamma_{k\ell}\, f_k\, f_\ell \tag{30}$$

where $k = 1,2,3,\ldots,N$

$\ell = 1,2,3,\ldots,N$

The expressions for $\alpha_{k\ell}$, $\beta_{k\ell}$ and $\gamma_{k\ell}$ are definite integrals given in Appendix B. The evaluation of these definite integrals will be performed in Chapter IV.

In Equations (28), (29) and (30), it is obvious that

$$\frac{\partial V}{\partial \dot{f}_k} = 0$$

and

$$\frac{\partial T}{\partial f_k} = 0$$

Therefore Lagrange's Equations (20) can be rewritten as

$$\frac{d}{dt}\left\{\frac{\partial T}{\partial \dot{f}_j}\right\} + \frac{\partial U}{\partial f_j} - \frac{\partial V}{\partial f_j} = 0 \tag{31}$$

Substitution for T, U and V from Equations (28), (29) and (30) into Equation (31) yields

$$\frac{d}{dt}\left[\alpha_{j\ell}\dot{f}_{\ell} + \alpha_{kj}\dot{f}_{k}\right] + \left[(\beta_{j\ell}f_{\ell} + \beta_{kj}f_{k}) + (\gamma_{j\ell}f_{\ell} + \gamma_{kj}f_{k})\right] = 0 \qquad (32)$$

Using the summation properties of the indices and the symmetry properties of the elements of α, β and γ, Equation (32) can be rewritten as

$$2\alpha_{k\ell}\ddot{f}_{\ell} + 2\beta_{k\ell}f_{\ell} + 2\gamma_{k}f_{\ell} + 2\gamma_{k\ell}f_{\ell} = 0$$

or

$$\alpha_{k\ell}\ddot{f}_{\ell} + (\beta_{k\ell} + \gamma_{k\ell})f_{\ell} = 0 \qquad (33)$$

Introducing the in-plane force amplitude parameters c and d into the mean and periodic components of the load (see Appendix C), $\gamma_{k\ell}$ can be written as

$$\gamma_{k\ell} = (c + d\cos\lambda t)\Gamma_{k\ell} \qquad (34)$$

where $\Gamma_{k\ell}$ is defined in Appendix C. Thus Equation (33) can be written in the form

$$\alpha_{k\ell}\ddot{f}_{\ell} + [\beta_{k\ell} + (c + d\cos\lambda t)\Gamma_{k\ell}]f_{\ell} = 0 \qquad (35)$$

where $k, \ell = 1,2,\ldots,N$.

Equation (35) represents a set of simultaneous equations, which can be further written in matrix form as

$$[\alpha]\{\ddot{f}\} + [\beta]\{f\} + c[\Gamma]\{f\} + d\cos\lambda t[\Gamma]\{f\} = \{0\} \; . \qquad (36)$$

Introducing the underline notation for square matrices $[\alpha]$, $[\beta]$, $[\Gamma]$ and column matrices $\{f\}$, and $\{0\}$, so that

$$[\alpha] = \underline{\alpha}$$

$$[\beta] = \underline{\beta}$$

$$[\Gamma] = \underline{\Gamma} \quad \text{and} \quad \{f\} = \underset{\sim}{f}$$

Equation (36) can be written as

$$\underline{\alpha}\, \ddot{\underset{\sim}{f}} + [\underline{\beta} + (c + d \cos \lambda t)\underline{\Gamma}]\, \underset{\sim}{f} = \underset{\sim}{0} \tag{37}$$

The square matrix $\underline{\alpha}$ is obtained from the kinetic energy of the system and is known as the Inertia or Mass matrix. Matrices $\underline{\beta}$ and $\underline{\Gamma}$ are derived from the potential of the system. The matrix $\underline{\beta}$ is the stiffness matrix. The elements of these matrices are constants and will be obtained from the energy expressions in Chapter IV. Equations (37) are the governing equations for dynamic stability of a parametrically excited system. The governing equations for special cases of this problem can be obtained by setting various combinations of the matrices to zero in Equation (37).

Special Cases of the Parametric Excitation Problem

a. Free Vibration Problem

If the external mean load and the alternating loads are removed, the dynamic stability problem reduces to a free vibration problem. The elimination of the force amplitude parameters c and d in the mean and periodic components of load respectively, from Equation (37) results in

$$\underline{\alpha}\, \ddot{\underset{\sim}{f}} + \underline{\beta}\, \underset{\sim}{f} = \underset{\sim}{0} \tag{38}$$

Considering the motion to be simple Harmonic, a solution of this equation gives the natural frequencies of free vibration. Details will be presented in Chapter IV.

b. Buckling Problem

For static buckling there is no oscillatory motion. Therefore the inertia forces and applied alternating loads can be eliminated. As a result, Equation (37) takes the form:

$$[\underline{\beta} + c\ \underline{\Gamma}]\underset{\sim}{f} = \underset{\sim}{0} \tag{39}$$

This equation describes an Eigenvalue problem. The values of c which satisfy Equation (39) are called the Eigenvalues of the problem. The smallest eigenvalue will correspond to the critical buckling load. When there is no edge crack in the plate, or when the crack is of relatively short length, the buckling will occur only due to an applied compressive load. For a crack of sufficiently large length, however, both local buckling under a tensile load and global buckling under a compressive load can occur. The analysis of the tensile buckling problem will be performed in Chapter IV.

c. Free Vibration under Mean Load

In this case, the plate subjected to static tensile load vibrates in the transverse direction, and the aim is to determine the natural frequencies of vibration under a fixed load. Setting the force amplitude parameter, d, for the alternating load equal to zero in Equation (37), the governing equation for this specific case takes the form

$$\underline{\alpha}\ \ddot{\underset{\sim}{f}} + (\underline{\beta} + c\ \underline{\Gamma})\underset{\sim}{f} = \underset{\sim}{0} \tag{40}$$

The detailed solution to this equation will be described in Chapter IV.

d. Dynamic Stability Problem

Here, the plate is subjected to a mean tensile load and is also excited parametrically by an alternating load. For a given combination of mean load, P_0, and alternating load, P_1, resonant type oscillations of the plate can occur at certain values of excitation frequency. The plate is then said to be dynamically unstable, and the response is governed by Equation (37). The matrices $\underline{\alpha}$, $\underline{\beta}$ and $\underline{\Gamma}$ in Equation (37) are square matrices with nonzero constant elements which will be obtained in Chapter IV.

The solution to the problem involves finding the regions of stability and instability in a parameter space; i.e., in terms of c, d and λ. Regions of unboundedly increasing amplitude are separated from the regions of stability by boundaries on which periodic solutions with periods T and 2T are developed [5]. The location of the boundaries in the parameter space will be determined in Chapter IV.

CHAPTER III

EXPERIMENTAL INVESTIGATION

Introduction

It was realised at the outset that an analytical investigation of the parametric excitation of a tensioned sheet with an edge crack would be difficult. Also, the extent to which a simplified mathematical representation could be expected to exhibit actual behavior was an open question. Since the problem was to be solved analytically in three different stages, it was decided to conduct experiments which checked the results at each stage. These stages were as follows:

a) The first stage was to perform the free vibration modal analysis. The modes obtained from this analysis were used in the analyses carried out in the next two stages.

b) The second stage was to obtain the in-plane stress distribution and to solve the static buckling problem. A computational program developed in reference [21] was used to determine the in-plane nonuniform stress distribution. The values of stress intensity factors obtained from this program had been compared with results from solutions available in the literature [Ref. 21, p. 15], and had been found to be acceptable. The experiments for static local buckling were described in Reference 22. These results will also be given in this chapter.

c) The last stage was to solve the parametric excitation problem. The free vibration modes obtained from the first stage and the stress

distribution determined in the second stage were used in the investigation of this stage. Experiments were conducted to evaluate the analytical results obtained from this part of the investigation.

The details of the experimental investigations conducted for the free vibration and parametric excitation are presented in the sections which follow.

Free Vibration Problem

If a transverse periodic excitation is applied to the cracked plate, it will develop large amplitude oscillations in the vicinity of the natural frequency of free vibration. This is called a resonant condition. For an undamped system which passes through a resonance condition, a phase shift of 180° develops between the simple harmonically exciting force and the vibrating element. This characteristic phase shift can be used as a basis for determining the frequency at which resonance occurs. With damping present the determination is, of course, approximate. The lowest resonant frequency required here, however, can be determined with sufficient accuracy. The details of the investigation conducted are described in the subsequent sections.

Specimen

The same basic specimen was used for all experimental work conducted for the investigations of free vibration, buckling and dynamic stability. A 0.025 inch thick sheet of aluminum alloy 2024 - T3 was chosen for all tests. A desire to restrict element frequencies to be less than 100 Hz dictated the size of the specimen. A Raleigh-Ritz procedure was used to obtain a preliminary estimate of the lowest natural frequency of a

rectangular plate with two opposite edges clamped and the other two edges free. Previously published experimental work [23] indicated that the introduction of a crack parallel to opposite-supported edges reduces the natural frequency. On the basis of the preliminary calculations, the dimension parallel to the clamped edge was chosen as 4.4 inches and the other dimension, parallel to the free edge, was chosen to be 12 inches. The edge crack was simulated by the use of a narrow slot with a width of 3/32 inch (see Figure 6).

Test Facility

A diagram of the test facility used to conduct the free vibration experiment is shown in Figure 7. Two heavy aluminum blocks were rigidly clamped to a table. A (4 × 1-1/2 × 3/16 inch) channel section was clamped to the top of each of these blocks. The specimen, which was provided with 3/8 inch thick aluminum end plates to introduce the clamped edge support, was in turn attached to the flanges of the channel section. The other two sides were free of constraint.

The excitation was provided by an electromagnetic shaker of ±25 lbs. range. It is designated as MB Model PM-35 by the manufacturer, MB Electronics. An oscillator manufactured by Yokogawa-Hewlett-Packard (Model 203A) was used to control the shaker frequency. The power was supplied to the oscillator, and a power amplitude was connected between the oscillator and the electromagnetic shaker. This controlled the magnitude of the alternating force provided by the shaker. The power amplifier used is designated as Model 2125 MB by the manufacturer, MB Electronics. A combination accelerometer and load cell was attached to the moving element of the shaker. During these tests the load cell was brought in contact

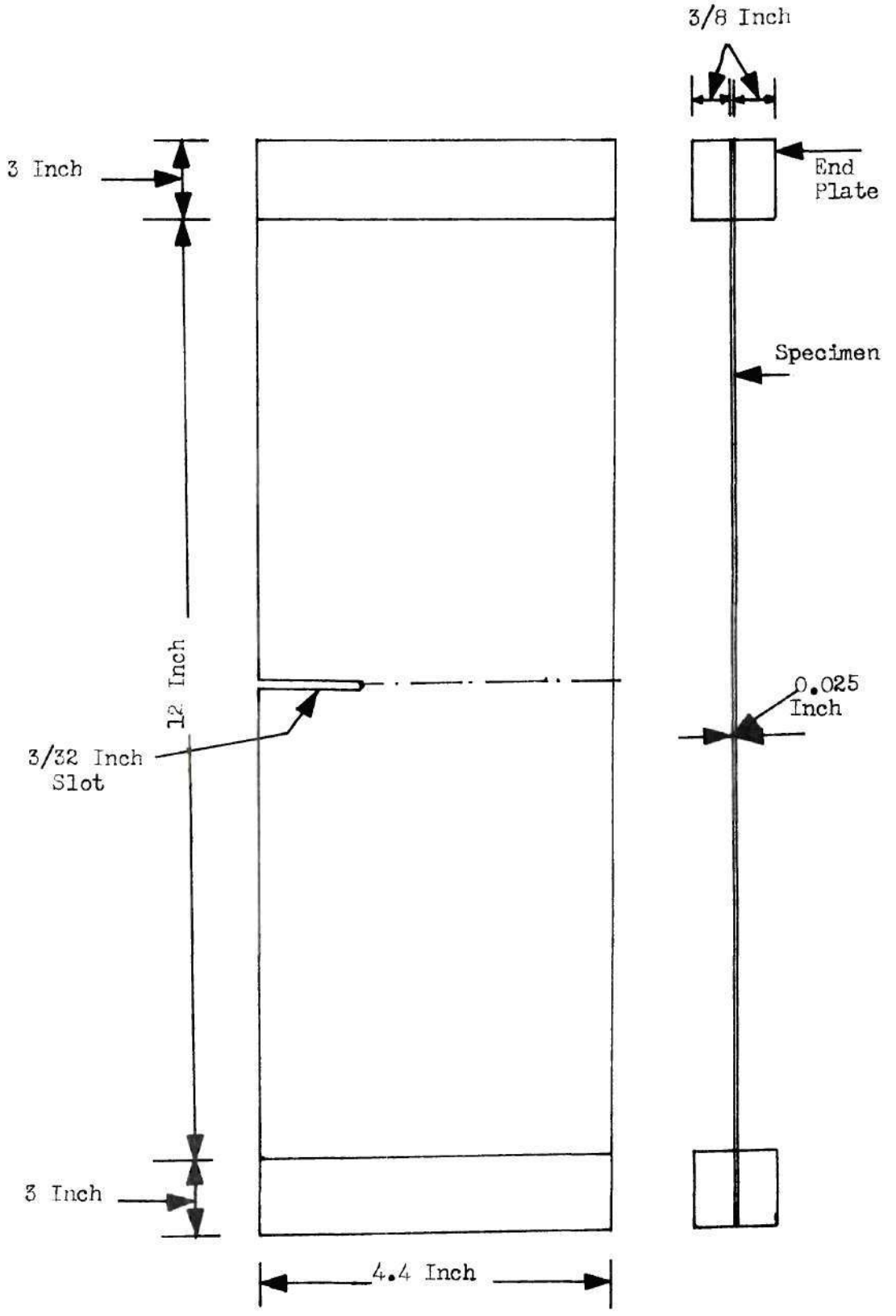

Figure 6. Specimen for Free Vibration Test.

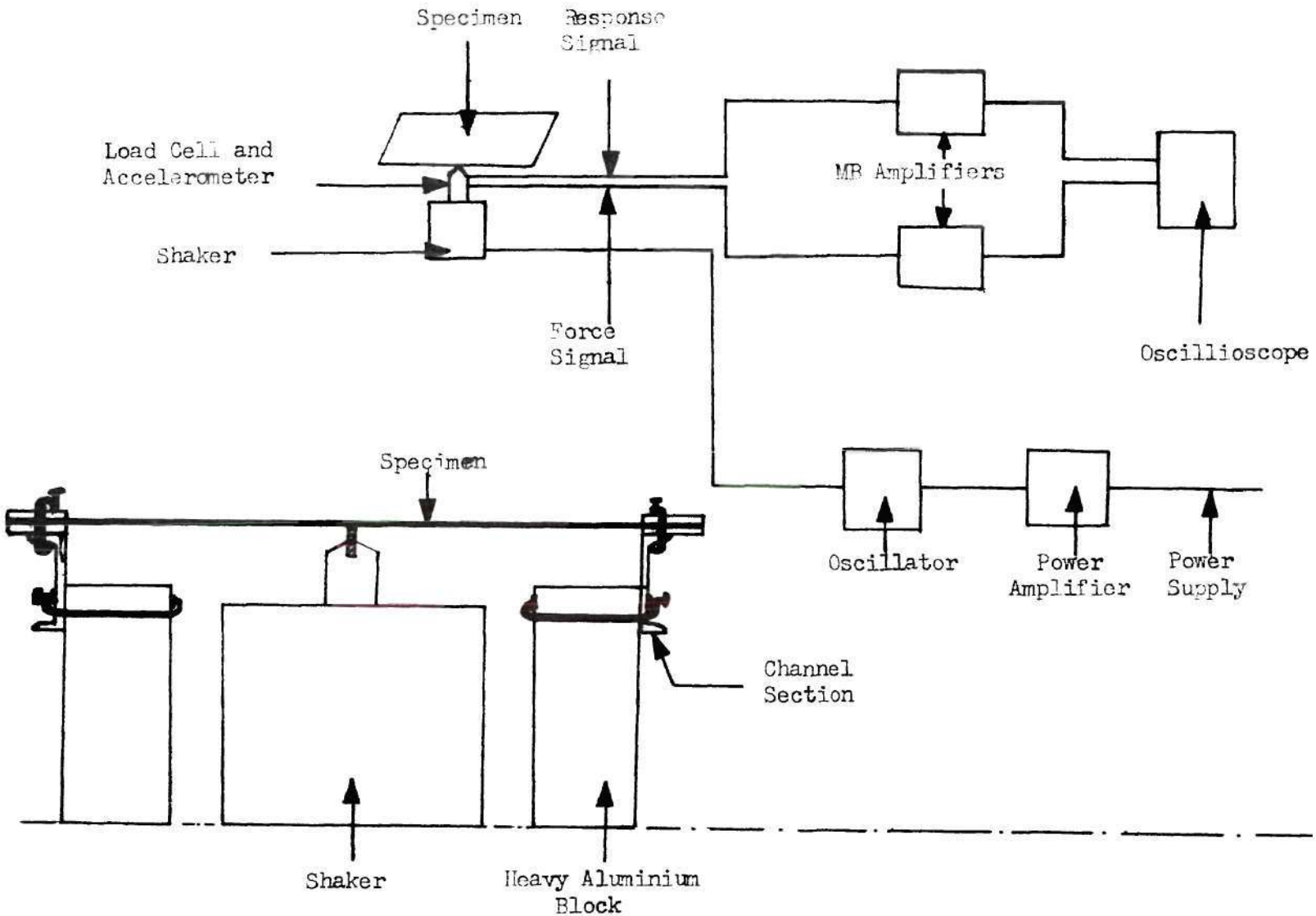

Figure 7. Free Vibration Test Facility.

with the specimen surface. The accelerometer measured the response in terms of acceleration of the specimen surface. The output from the load cell gave the history of the exciting transverse force. The outputs from the load cell and accelerometer were amplified by connected amplifiers which were manufactured by MB Electronics. The amplified signals were fed to the two channels of an oscilloscope. The force and acceleration signals were displayed on the vertical and horizontal axes, respectively. The oscilloscope used was manufactured by Hewlett-Packard and is designated as Model 1200 A.

Test Procedure

As described before, the characteristic phase shift between the exciting force and acceleration of the vibrating specimen provides the basis for determining the frequency at which the element exhibits a resonance type behavior. When the amplified force and response signals are fed into the vertical and horizontal inputs of an oscilloscope, the trace of force versus response with damping is an ellipse as shown in Figure 8. The change in sign of the in-phase component occurs when the phase shift becomes 180°, which in turn is an indication of transition through the natural frequency.

The frequency on the oscillator was varied while observing the trace on the oscilloscope. The oscillator frequency was recorded as the natural frequency of the specimen when the ellipse on the screen became vertical. The higher natural frequencies were recorded by increasing the oscillator frequency and observing the same kind of behavior on the oscilloscope. Both symmetric and antisymmetric modes were observed. The crack length was increased from 0 to 4 inches in increments of one

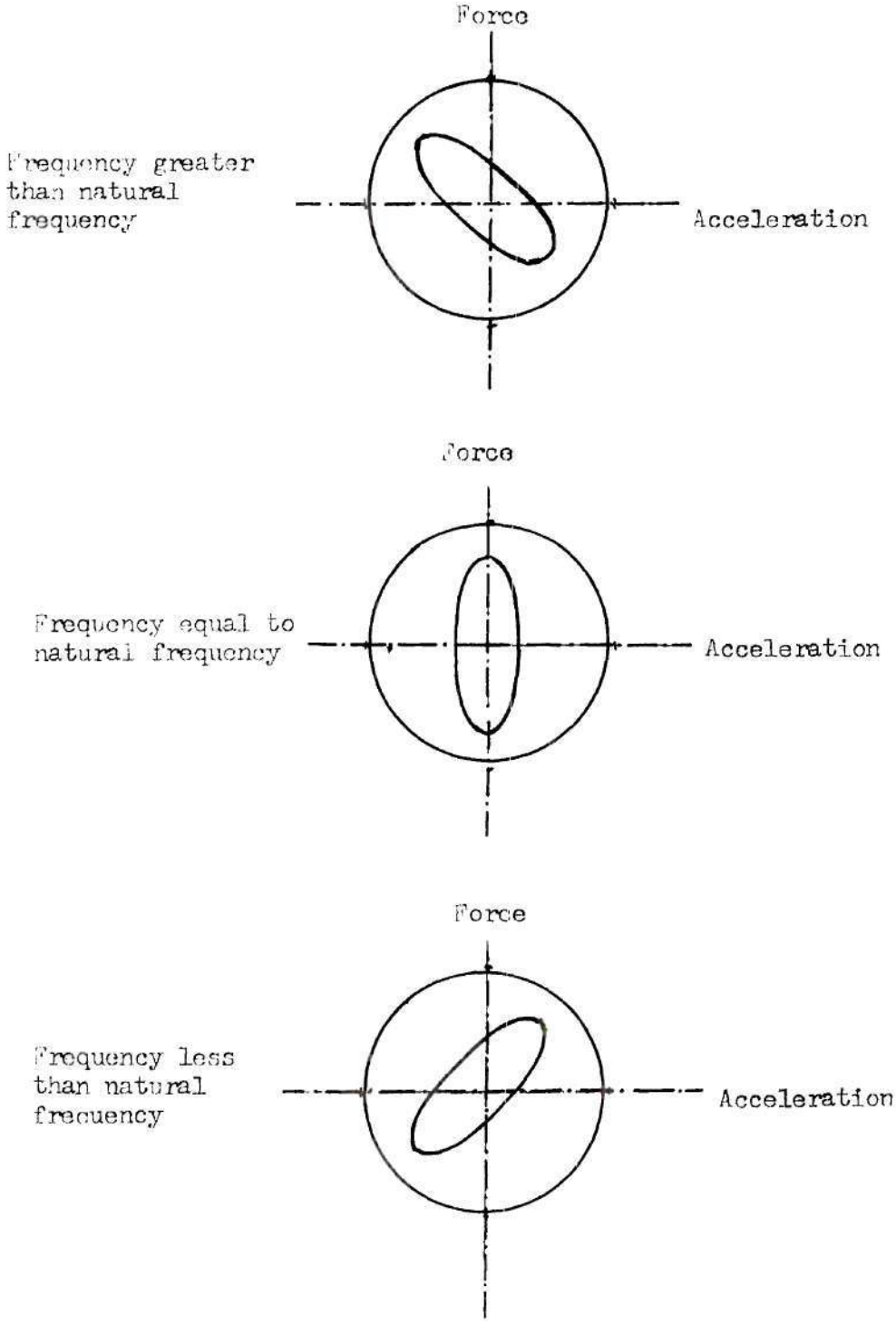

Figure 8. Force vs. Acceleration on Oscillioscope.

half inch. The experiment was repeated for each crack length.

Test Results

The free vibration frequencies corresponding to the first symmetric and first antisymmetric modes and various crack lengths are given in Table 1.

Table 1. Experimental Results for Free Vibration Frequencies

$\frac{a}{(a+b)}$	Free Vibration Frequency (Hz) First Symmetric Mode	First Antisymmetric Mode
0.0	37.5	87.5
0.2273	35.5	87.0
0.4545	34.25	86.0
0.5681	33.25	82.0
0.6818	31.50	76.0
0.7955	27.60	65.0
0.9091	23.0	59.0

Parametric Excitation

Introduction

For the parametric excitation experiments the specimen was subjected to a mean tensile load, P_0, and then a time dependent load, $P_1 \cos \lambda t$, was applied. For fixed values of P_0 and P_1, the specimen will exhibit a resonance type behavior at certain values of frequency of the time-dependent load. The determination of these transition frequencies is the objective to the experiments.

The first resonance occurs when the frequency of alternating load becomes approximately equal to the natural frequency of vibration of the specimen under the mean load. The frequencies associated with the resonance behavior define the boundaries of the so-called secondary region of dynamic stability. A second resonance behavior corresponding to what is described as the principal region occurs for frequencies of approximately twice the natural frequency.

In summary the experimental investigation of dynamic stability had as its objective the determination of frequencies of alternating load for which the specimen exhibited a resonance behavior.

Specimen

The analytical results of free vibrations were used in the analysis of the parametric excitation problem. The same basic specimen was, therefore, used for the dynamic stability experiments as had been used for the free vibration experiments. The 0.025 inch thick sheet of aluminum alloy 2024-T3 was used to produ-e a specimen of the same dimensions as for the free vibration specimen. Since a combination of distributed mean and alternating loads was to be applied along the fixed edges, 0.375 inch thick plates were bonded to both faces of the sheet at the fixed ends as indicated in Figure 9. These end plates were made from a plate stock of aluminum alloy 2024-T4. They were bonded with a room temperature curing epoxy. Two dowel pins were used at each end to insure proper alignment of the end plates on the sheet. The load was applied to the end plates through a pin inserted in a centrally located circular hole of radius 3/16 inch. In order to avoid propagation of the crack due to cyclic loading, the slot ended with a tip radius of 0.16

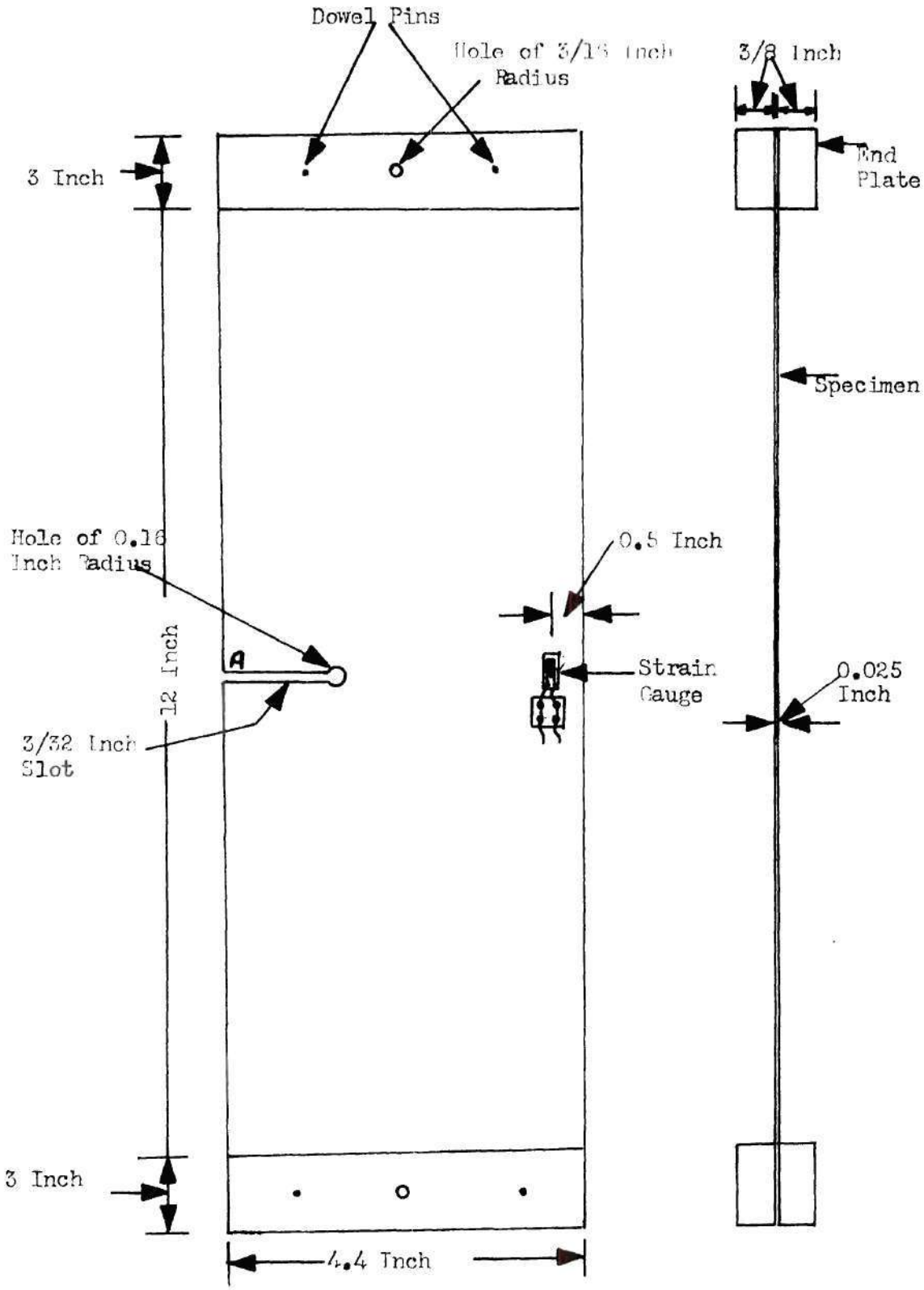

Figure 9. Specimen for Dynamic Stability Test.

inch. Two electrical resistance strain gauges were bonded to the sheet, back to back, as indicated in Figure 9. The strain sensitive axes of the gauges were parallel to the free edges of the specimen and were located at 0.5 inch inside the free edge.

Test Facility

The test facility used for the dynamic stability experiments is shown in Figure 10. A reinforced concrete base of the test frame was isolated from the ground by four large coil springs. The frame consisted of two vertical members made from steel I sections, and a cross bar at the top made from a steel H section. Another cross bar made from aluminum stock is attached 2.3 feet from the base and its center was connected to the oscillating element of the shaker.

The mean load was applied through a screw mechanism which was housed at the center of the top cross member. The alternating load was applied through an electromagnetic shaker of ±50 lbs. capacity. The shaker used was manufactured by MB Electronics and is designated as MB Model (11-1). It was fixed to the concrete base and its oscillating element was connected to the bottom cross member. The shaker control system consisted of a power supply, a d-c field supply, an oscillator and a power amplifier. The system is designated as Model T-112531 by the manufacturer, MB Electronics. The specimen was attached to the loading mechanism at the top through a clevis and a universal joint. It was attached at the bottom end to a clevis connected to the bottom cross bar. The magnitude of the mean load was determined by a load cell placed between the top clevis and universal joint.

The response of the specimen was indicated by measuring the output

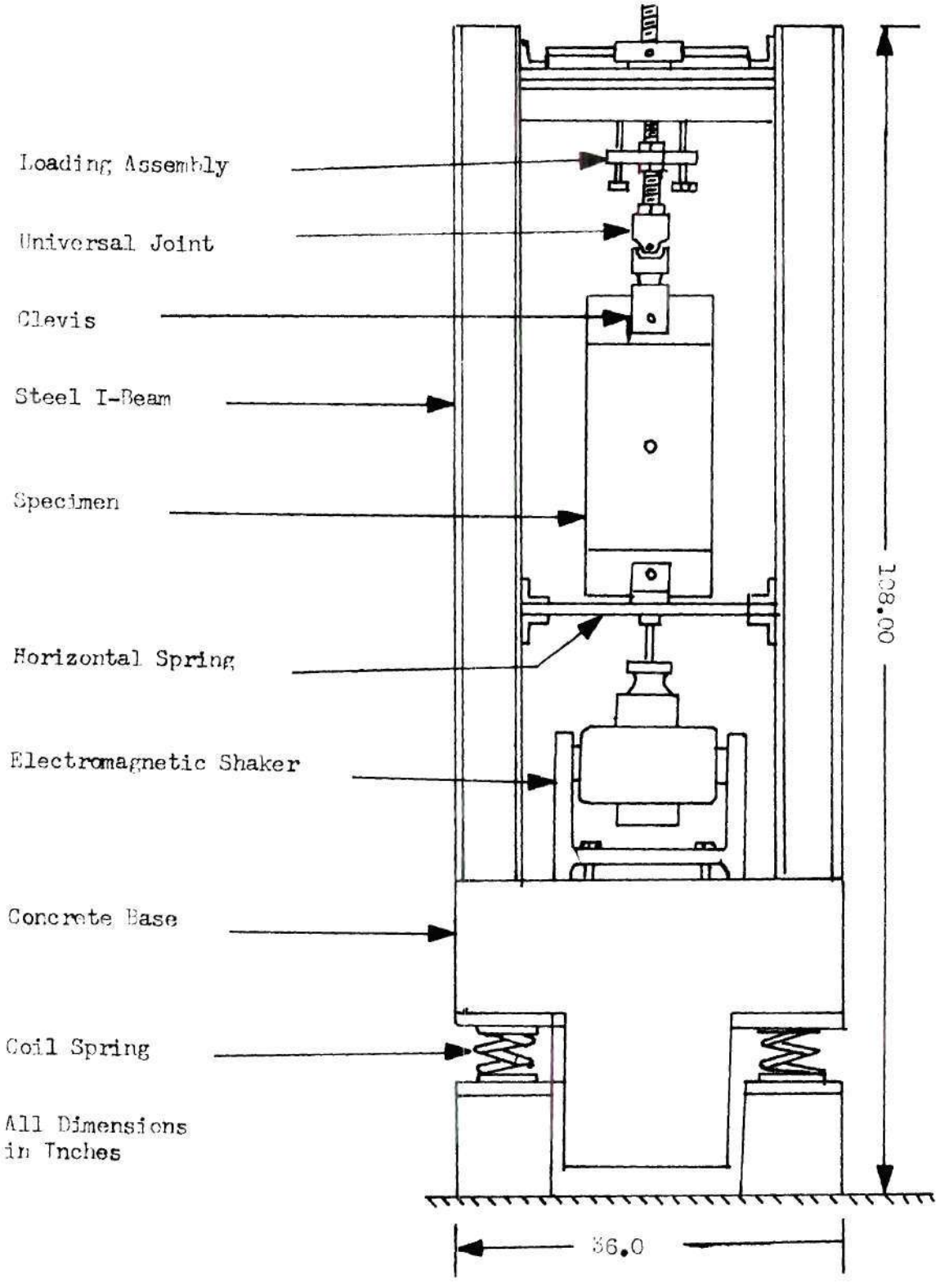

Figure 10. Dynamic Stability Test Facility.

from two electrical-resistance strain gauges (shown in Figure 9). These gauges formed the two adjacent sides of a Wheatstone bridge. Two gauges bonded to an unstressed aluminum sheet were inserted in the remaining arms of the bridge. The bridge for the sheet response and the bridge from the load cell were connected to Hewlett-Packard carrier pre-amplifiers (Model 8805A), and the signals generated were fed to two channels of a Hewlett-Packard recorder (Model 7702 B).

Another cross bar was clamped to the flanges of the vertical members. A micrometer mounted on this cross bar was used to measure the magnitude of the transverse deflections of point A (see Figure 9) of the vibrating plate.

Test Procedure

Prior to initiation of testing, the load cell was calibrated. Weights were applied to the top clevis and output readings were recorded on one channel of the Hewlett-Packard recorder. A calibration curve was then prepared from the load -- output data.

The dynamic stability tests were then commenced. The specimen was inserted in the facility and connected to the recorder. A mean load was first applied and then, after connecting the shaker to the lower cross-bar, an alternating load was introduced. The frequency of the alternating load was increased. The frequency of the alternating load was increased slowly from zero until a resonance type behavior was exhibited by the specimen. The frequency of the initiation of this response was then recorded as the lower boundary of the secondary region of instability. The upper boundary frequency for this region was obtained by increasing the frequency to a value above the secondary region. The

frequency was then decreased until resonance was again observed. This transition frequency was identified as the upper boundary of the secondary region.

The transverse deflections associated with the secondary region were measured by the micrometer when the amplitude of these oscillations, as indicated by the recorder, was a maximum. The deflection was determined by noting the initial reading for the specimen when it was not vibrating, and then taking the final reading by advancing the micrometer spindle until contact was made with the vibrating specimen. The difference between the contact readings, before and after resonance, was used as a measure of the deflection.

The frequency of the alternating load was then increased until large amplitude oscillations occurred. These oscillations were observed to occur at a frequency of one half the frequency of the applied load. This resonance corresponded to the lower boundary of the principal region of instability. The location of the upper boundary of the principal region was determined in the same manner as the upper boundary of the secondary region. Again the magnitude of the transverse deflections was measured by use of the micrometer.

To map the parameter space for the specimen, it was necessary to repeat the test procedure described for a range of values of alternating load. After completing the required tests for one crack length, the crack length was increased and the experiments were repeated. Test data for a series of crack lengths were obtained in this manner.

Test Results

The frequencies corresponding to the lower and upper boundaries of

the secondary and principal regions of dynamic stability are given in Table 2. For each crack length, a mean load of 25 lbs. was used. For each crack length, a mean load of 25 lbs. was used. Alternating loads of 4, 8, 12 and 16 lbs. were investigated. Crack length values from zero to 3.1 inches are given.

At a crack length of 2.8 inches, the crack propagated along the center line of the specimen about 0.2 inches. This happened when the last set of readings were being taken for that crack length. The crack length was then increased to 3.1 inches and the experiments were recommenced. At this crack length, and for an alternating load of 16 pounds the crack propagated during the experiment. The crack extended 0.6 inch along the direction of the crack and then turned through an angle of about 45° and extended an additional 0.2 inch. Since it was no longer possible to conduct tests without crack extension, testing was terminated.

The transverse deflections associated with the secondary and principal regions were measured for each crack length. These deflections were measured when the amplitude of oscillation, as indicated by the recorder, was a maximum. These amplitudes were only recorded when the specimen was subjected to an alternating load of 16 pounds. The dynamic stability results are given in Table 2, and results for the lateral deflections are presented in Table 3.

Static Buckling

Experiments were conducted to observe the behavior of localized buckling of the tensioned sheet with an edge crack. A detailed program with this objective is discussed in Reference 22. The specimen used was

Table 2. Experimental Results for Dynamic Stability

a. Principal-Region Boundaries, P_0 = 25 lbs.

P_1 / a/(a+b)	4	8	12	16
	Excitation Frequency (Hz)			
0.0	105.0, 109.5	100.0, 112.0	95.0, 115.0	89.0, 117.5
0.2273	104.0, 109.0	99.5, 113.0	93.0, 114.5	86.0, 116.0
0.4545	102.0, 107.0	96.0, 111.0	89.0, 113.0	83.0, 114.0
0.5000	100.0, 106.0	95.0, 108.5	88.0, 112.5	82.5, 114.0
0.5455	99.0, 105.0	94.0, 107.75	87.5, 111.0	81.0, 113.0
0.5909	97.0, 103.5	92.5, 107.5	86.0, 108.0	78.0, 111.0
0.6364	96.5, 103.0	91.0, 107.0	84.0, 107.0	76.0, 109.0
0.7046	92.0, 98.0	90.0, 100.0	86.0, 102.0	71.0, 84.0

b. Secondary-Region Boundaries, P_0 = 25 lbs

P_1 / a/(a+b)	4	8	12	16
	Excitation Frequency (Hz)			
0.0	53.0, 53.0	51.0, 54.0	47.5, 54.0	45.5, 53.5
.2273	52.0, 53.0	50.5, 53.0	47.5, 53.0	45.5, 52.5
.4545	51.0, 51.5	48.5, 51.5	46.75, 52	43.5, 52.0
0.5000	50.0, 51.5	48.0, 51.0	45.5, 50.5	43.0, 50.5
.5455	49.5, 51.0	47.5, 50.5	45.0, 50.5	42.5, 50.5
.5909	48.5, 50.0	46.0, 49.5	43.5, 49.5	41.0, 49.5
.6364	47.0, 49.5	44.5, 49.0	42,5, 48.5	40.0, 49.0
.7046	46.0, 49.0	42.5, 48.5	38.5, 48.0	36.0, 47.5

Table 3. Lateral Deflections, P_o = 25 lbs, P_1 = 16 lbs

Instability Region	Lateral Deflection (Inches)	
a/(a + b)	Secondary Region	Principal Region
0.0	0.13	0.260
0.2273	0.15	0.275
0.4545	0.183	0.335
0.5000	0.215	0.300
0.5455	0.233	0.400
0.5909	0.240	0.400
0.6364	0.260	0.430
0.7046		

made from the same type of aluminum alloy sheet as used for the specimens for the free vibration and parametric excitation tests. It was an aluminum alloy 2024-T3 sheet with a thickness of 0.025 inch. The geometric boundary conditions and width of the specimen were also the same as used for other two tests. The length, however, of the buckling specimen was 22 inches as compared to 12 inches for the specimens used for the free vibration and parametric excitation. The analytical investigation for the buckling problem was carried out with a length of 12 inches. Since it was observed that the analytical stress distribution up to a crack length of 3.5 inches was a uniform tension in portions of the plate away from central 12 inch portion, and since the localized compressive stress is the cause of local buckling of the tensioned sheet

with an edge crack, an attempt was made to compare the experimental results of a 22 inches long specimen with the analytical buckling load results of the 12 inch specimen.

Two-electrical resistance strain gauges, applied back-to-back in expected compressive region were used to read the strains on the two surfaces while the specimen was subjected to tensile loading. The difference in the two strain gauge outputs is a measure of the local bending strain.

The specimen was loaded in an Instron testing machine with load increments and a load range which depended upon the length of the crack. All of the load-vs-strain difference data obtained for the specimen tested for various crack lengths is presented in Reference 22.

Southwell plots and modified Southwell plots or so called Lundquist plots were obtained from load-vs-strain difference data. The test procedure used and the analysis of data obtained by this method are discussed in detail in References 24 and 25.

The tensile loads deduced for local buckling of specimens with various crack length are given in Table 4.

Table 4. Experimental Results for Buckling Loads

$a/(a+b)$	Buckling Load (lbs, Tensile)
0.4545	∞
0.5682	96.0
0.6818	49.0
0.7955	40.0

CHAPTER IV

ANALYTICAL INVESTIGATION

Introduction

In the second chapter, the development of the governing differential equations for the general parametric excitation problem and the special cases of free vibration, buckling and free vibration under mean initial load were discussed. All these equations were derived from a set of simultaneous differential equations and were written in matrix form. The procedure adopted to develop these equations was based on the use of Lagrange' Equations, and the method of assumed modes. As the name implies, the first step of the method involves the generation of modes which can be used to solve each of the problems described above. Often, it proves convenient to utilize the modes from the solution of the free vibration problem for the given structural system. These modes can then be used to solve related problems for the system. This is the technique employed in the present investigation.

In the problem of interest, the presence of the crack causes the stress distribution to be nonuniform. Since the stress components appear in the integrands of some of the definite integrals which appear as coefficients in Equation (37), the stress distribution must be determined for the cracked plate. The details of this analysis are also presented in this chapter.

Modal Analysis

Mode shapes for free vibrations may be determined in several ways. Once the mode shapes for this specific problem are known, they can be used for the analysis of the other problems of interest discussed in the previous sections. In this dissertation, three methods have been examined. One involves the use of trigonometric functions. A second is based on the construction of acceptable polynomial functions. The last uses a finite element technique.

Trigonometric Functions

To account for the geometric features due to the presence of the edge crack, trigonometric functions which included a crack tip singularity of the proper order were considered (see, for example, the work of Williams [26]). A polar coordinate system was introduced for the convenient application of the series developed. A sketch of the analytical model for the problem in polar coordinate system is shown in Figure 11.

For the case of symmetric deflections, a sum of functions was chosen as

$$\bar{w} = [(\frac{\bar{y}}{\ell})^2 - 1]^2 [c_1 + c_2 r \cos 2\theta + c_3 r^{\frac{3}{2}} \sin \frac{\theta}{2}] , \qquad (41)$$

where c_1, c_2 and c_3 are unknown functions of time, t.

The terms in the first bracket satisfy the conditions of zero deflection and zero slope $(\frac{\partial \bar{w}}{\partial \bar{y}})$ along the clamped edges of the plate, while the second bracket includes a term $r^{\frac{3}{2}} \sin \frac{\theta}{2}$, which introduces a singularity of the proper order in the bending moment at the crack tip.

An antisymmetric shape may also be developed. For this deflection shape, a function was chosen in which

$$\bar{w} = [(\frac{\bar{y}}{\ell})^2 - 1]^2 [c_4 r^{\frac{3}{2}} \cos \frac{\theta}{2} + c_5 r \sin \theta], \tag{42}$$

where c_4 and c_5 are unknown functions of time, t.

The kinetic energy, T, and the internal energy, U, can be determined for the cracked plate by the use of appropriate definite integrals expressed in terms of polar coordinates. By use of either Equation (41) or Equation (42), expressions for T and U can then be obtained in terms of the time-dependent coefficients. When these results are inserted into Lagrange's Equations, a system of second order ordinary differential equations is generated. By considering the case of simple harmonic motion, the time variable is eliminated, and the following system of algebraic equations is obtained:

$$\sum_{j=1}^{3} (\alpha_{ij} - \omega^2 \beta_{ij}) k_j = 0 \quad i=1,2,3 \tag{43}$$

where ω is the free vibration frequency in radians per second, and K_j is an eigenvector which represents the amplitude of the deflection function.

The corresponding characteristic determinant can be written as

$$|\alpha_{ij} - \omega^2 \beta_{ij}| = 0 \tag{44}$$

Equation (44) can be solved for the eigenvalues, ω, which can be used to determine the eigenvectors. These eigenvectors when normalized represent

the relative magnitude of the unknown time dependent c_i's in the assumed mode shapes as given by Equation (41). For each eigenvalue, there corresponds a set of eigenvectors. Knowing the mode shape or deflection function, its derivatives can be computed, and the integrals defined in Equations (28) and (29) can be computed.

Polynomial Functions

Here again, for convenience, a polar coordinate system may be chosen for the analysis (see Figure 12). A polynomial can be constructed to represent a mode shape which specifies the fixed end boundary conditions and describes the geometric features due to presence of the crack.

For symmetric deflections, approximation functions of the following polynomial form may be chosen:

$$\bar{w} = [(\frac{\bar{y}}{\ell})^2 - 1]^2 [c_6 + c_7(r)^{\frac{3}{2}} + c_8 r^{\frac{3}{2}} \theta^2] \qquad (45)$$

where c_6, c_7 and c_8 are unknown functions of time, t.

The terms in the first bracket satisfy the conditions of zero deflection and zero slope at the clamped edges and the term, $r^{\frac{3}{2}} \theta^2$, in the second bracket introduces a singularity of proper order in the bending moment at the crack tip.

For the antisymmetric case, a deflection function may be chosen as

$$\bar{w} = [(\frac{\bar{y}}{\ell})^2 - 1]^2 [c_9 r^{\frac{3}{2}}\theta + c_{10} r^{\frac{3}{2}} \theta^3] \qquad (46)$$

where c_9 and c_{10} are unknown functions of time.

Using the forms of T and U, as given by Equations (28) and (29), applying the Lagrange's Equations (31), and considering simple harmonic

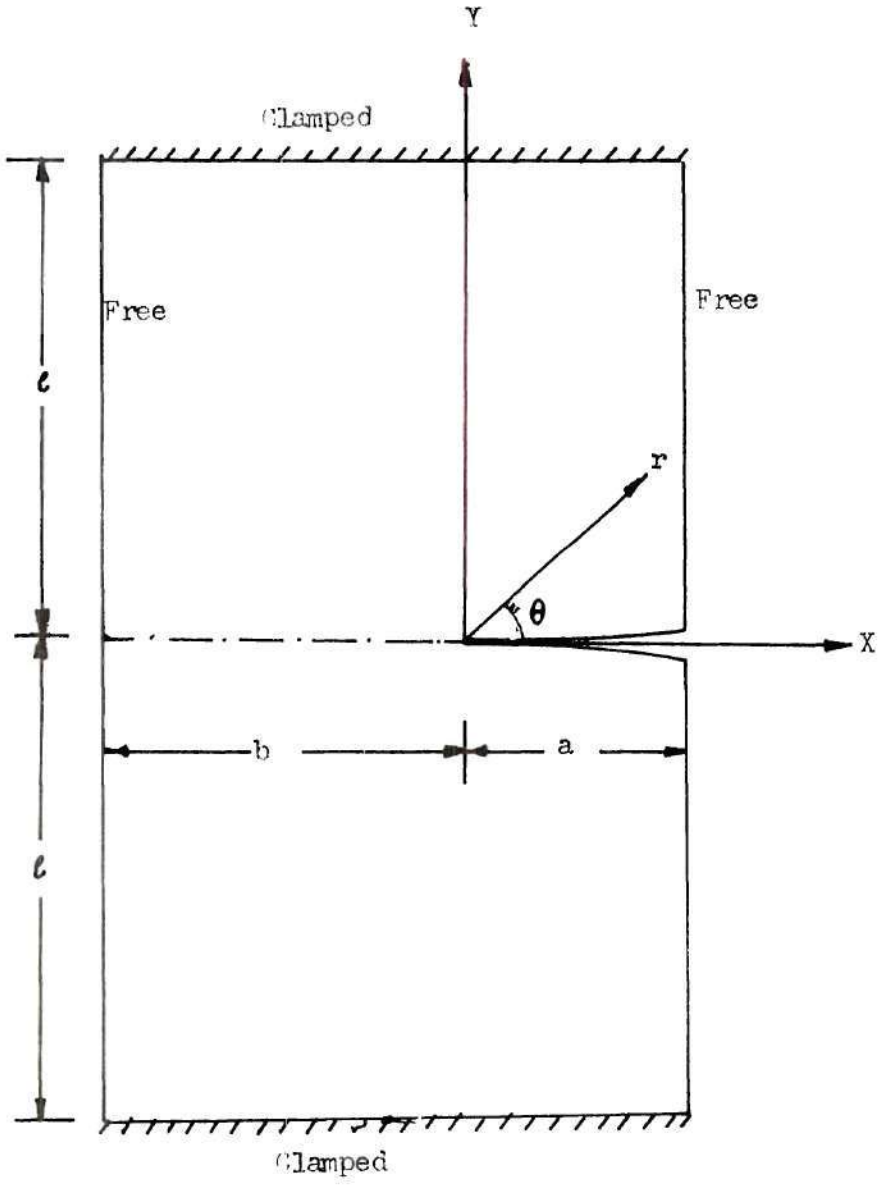

Figure 11. Analytical Model for Trigonometric Functions Solution.

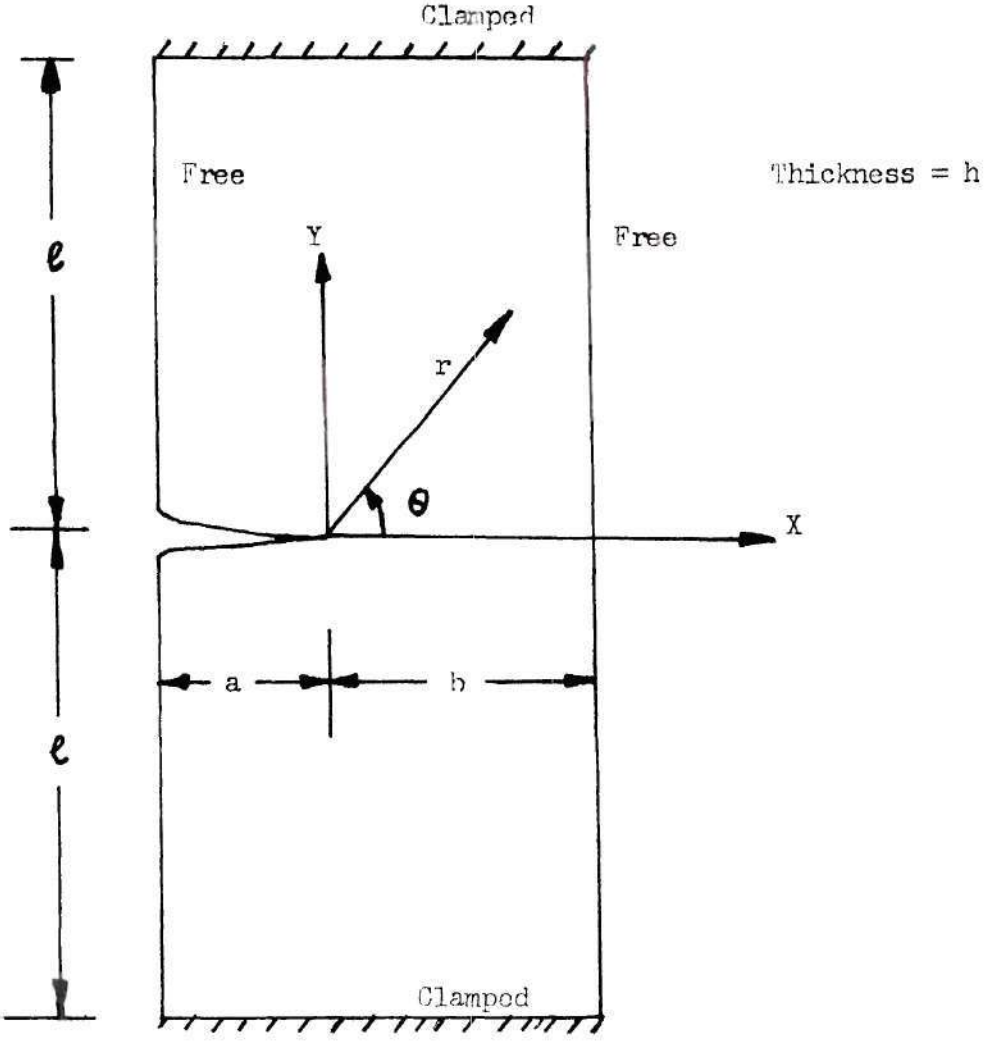

Figure 12. Analytical Model f or Polynomial Functions Solution.

motion, the characteristic determinant for free vibration eigenvalue problem is again of the form of Equation (44). The determination of eigenvalues and eigenvectors proceeds as before for the determination of the required functions for an assumed mode analysis. Thus, the free vibration mode shapes can be used in the computation of the integrals defined in Equations (28) and (29).

The computational work outlined above was carried out by Lukaart [12], using both the trigonometric and polynomial functions. He applied numerical integration techniques for the computation of the required integrals. Free vibration frequencies and corresponding eigenvectors were obtained for various crack lengths. To evaluate this method of analysis an experimental program was conducted to obtain the free vibration frequencies (details are given in Chapter III). The experimental and theoretical results are presented in Table 5.

Table 5. Experimental and Computed Frequencies

	Free Vibration Fundamental Symmetric Frequency in Hz		
a/(a + b)	Polynomial Function	Trigonometric Function	Experiment
0.0	-	-	37.5
0.2273	39.3	38.5	35.5
0.4545	38.8	38.8	34.25
0.5681	38.5	38.7	33.25
0.6818	37.0	38.5	31.50
0.7955	36.5	38.2	27.60
0.9091	-	-	23.0

An examination of the results in Table 5 reveals that the theoretical data obtained by using the above two methods were quite poor as compared with the experimental values. Therefore, the free vibration mode shapes constructed by trigonometric and polynomial functions were not used for the solutions of the buckling and dynamic stability problems. As an alternative, a finite element method was considered for the free vibration modal analysis. The application of this method is described in the next section.

Finite Elements

The finite element method [27, 28] and its application [29] to the free vibration problem is discussed in this section. In the displacement approach commonly used the continuum is subdivided into a number of finite elements. The type of continuity requirements between the adjacent elements depends upon the type of problem to be solved. A suitable element displacement function is then derived in terms of the unknown nodal displacements. This function depends upon the location of the element and defines uniquely the state of displacement within the element. The strain-displacement and stress-strain relations are introduced to develop relations which describe the stiffness of the elements (stiffness matrices). After using an appropriate assembly procedure, it is finally possible to express external forces in terms of the unknown nodal displacements of the complete structure as follows:

$$\{F\} + \{R\} = [K]\{\delta\} \tag{47}$$

In the above formulation forces due to initial strains and stresses are neglected. $\{F\}$ is a column matrix of elements which represent nodal

forces. These are approximately equivalent in effect to any distributed loads that are present. The column matrix $\{R\}$ consists of elements which represent externally applied nodal forces. The matrix [K] is a square matrix with constant elements which depend upon the geometric features of the plate elements and the properties of the structural material. This is called the stiffness matrix of the structure. The column matrix $\{\delta\}$, is called the nodal displacement vector and its elements consist of the unknown nodal displacements.

In the free vibration problem the externally applied nodal forces $\{R\}$, are absent and the distributed forces, $\{F\}$ are replaced by inertia forces of the form, $[M]\{\ddot{\delta}\}$. With a consideration of simple harmonic motion, Equation (47) reduces to the form

$$[[K] - \omega^2[M]]\{\bar{\delta}\} - \{0\} \tag{48}$$

where ω is free vibration frequency.

The elements of column matrix, $\{\bar{\delta}\}$, represent the amplitude of the unknown nodal displacements. Matrix [M] is called the inertia or mass matrix. This is a square matrix if the system is continuous and is called the consistent mass matrix. If the mass is considered to be lumped at the nodes, the mass matrix becomes diagonal.

Equation (48) represents an eigenvalue problem. The eigenvalues, ω, of the problem are determined from the characteristic determinant

$$|[K] - \omega^2[M]| = 0 \tag{49}$$

The set of eigenvectors, $\{\bar{\delta}\}$, corresponding to each eigenvalue is obtained by substituting the eigenvalue into Equation (48).

In the problem of free vibration it is simple and convenient to use a rectangular element. The unknown nodal displacement at each node then consist of the transverse displacement, w, and the angular displacements, θ_x and θ_y, about axes parallel to the X and Y axes respectively. To maintain continuity in slope at the interface between the elements results in mathematical and computational difficulties. However, it is relatively simple to satisfy the continuity of w along the interfaces of the elements and the continuity of slopes at the nodes. For a rectangular element an element displacement function can be assumed in the following form

$$w = \alpha_1 + \alpha_2 x + \alpha_3 y + \alpha_4 xy + \alpha_5 x^2 + \alpha_6 y^2 + \alpha_7 xy^2 + \alpha_8 y^3 + \alpha_9 x^2 y + \alpha_{10} x^3 + \alpha_{11} xy^3 + \alpha_{12} x^3 y \ . \tag{50}$$

Based on the finite element representation described above, a computational program for the free vibration modal analysis of structural members has been developed in STRUDL vol. II [29].

An analytical investigation of the free vibration modal analysis of cracked structures was performed in Reference 8. There, a comparison of eigenvalues and eigenfunctions for a simply supported cracked plate was made between two different types of analyses. In one analysis the crack tip singularity was ignored. In the second analysis the proper order of the crack tip singularity was incorporated in the computations. A comparison of the results indicated that the eigenvalues and eigenfunctions were essentially the same. The bending moments and hence the stress distributions were, however, quite different, adjacent to the

crack tip.

In the investigation described here the smallest eigenvalue and its corresponding eigenfunction were of primary interest; i.e., the dynamic behavior rather than the stress distribution was the topic of concern. No effort was made, therefore, to imbed a singularity element at the crack tip and STRUDL was used for the modal analysis.

Due to symmetry, only the upper half of the plate was considered. The plate was divided into a number of rectangular elements (in STRUDL, rectangular elements for plate bending are designated as BPR elements). Computations were made for several element sizes. The smallest number of elements used was ten. Good convergence in the results was obtained when thirty elements were used. The final form of the finite element grid used is shown in Figure 13.

The computational input data consisted of material properties, boundary conditions, and designation and location of the elements. The inertia matrix used was a lumped rather than consistent. The nodes 1 through 7 and 36 through 42 were rigidly supported initially. Then, to introduce the effect of the crack and to distinguish between symmetric and antisymmetric modes, an appropriate number of nodes along the X-axis were released to permit the transverse deflection and/or rotation as needed. The first six frequencies of free vibration, both for symmetric and antisymmetric cases were given by the STRUDL output. For every frequency, the mode shape was obtained in terms of the normalized nodal displacements, w, θ_x and θ_y at each node. Various crack lengths were considered, and the first two free vibration frequencies for each length are given in the Table 6.

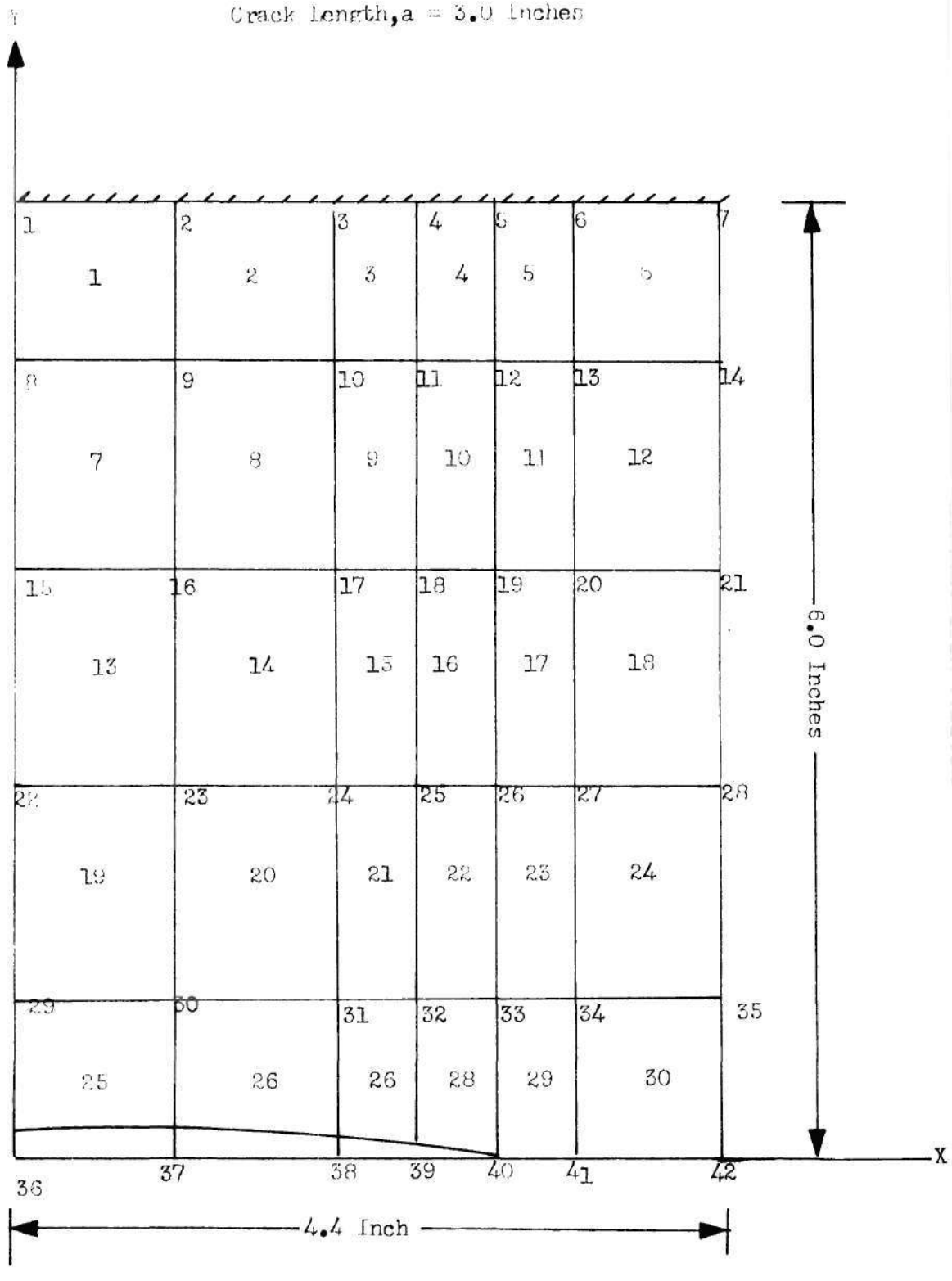

Figure 13. Finite Element Model for STRUDL.

Table 6. First Two Free Vibration Frequencies from STRUDL

a/(a + b)	Free Vibration Frequency (Hz)			
	Symmetric		Antisymmetric	
	Fundamental	Second	Fundamental	Second
0.0	37.08	72.05	103.50	159.27
0.2273	36.60	71.69	102.80	153.97
0.4545	34.91	71.13	97.04	135.10
0.5681	33.62	70.99	89.30	126.69
0.6818	32.29	70.96	78.99	122.71
0.7954	30.84	70.96	68.89	121.32
*0.0	37.85			

*Results obtained by using Raleigh-Ritz Method, where the solution function consisted of only fundamental modes.

Initial Stress Distribution

Introduction

The presence of the edge crack introduced a nonuniformity in the in-plane stress distribution, and the determination of the in-plane stress components, σ_x, σ_y and σ_{xy}, is required for obtaining the external potential as given in Equation (24). Initially the collocation method used by Gross, Strawley and Brown in Reference 30 was tried. The Airy stress function was represented by a sum of eigenfunctions derived originally by William in Reference 31. A number of equally spaced stations were chosen on the boundary (excluding the crack faces). The satisfaction of two boundary conditions at each of these stations yielded a set of linear

algebraic equations with the unknowns being the coefficients of the William's functions. A solution of these equations could then, in theory, be used to determine the stress distribution. In practice, however it was found that ill-conditioned matrices were developed and solution difficulties were encountered. This solution technique was, therefore, abandoned, and a finite element method was considered as an alternative.

Finite Element Method

The computational program used was developed by Anderson and Aberson [21]. In this solution procedure the crack tip singularity is introduced by the use of a special high-order cracked, finite element. This element incorporates terms of the William series, has a balance between actual degrees of freedom and nodal displacements, and has a convenient shape for interfacing with conventional elements. For the symmetric case, an 8 node element having sixteen degrees of freedom is used. This incorporates the first thirteen symmetric functions of the William series, and three displacement degrees of freedom associated with rigid-body displacement in the plane. For the antisymmetric case, a ten node element is used. This consists of the first eight symmetric and the first nine antisymmetric functions of the William's series and three rigid body displacements terms. Triangular elements were used for the rest of the plate (the grid is shown in Figure 14). The element stiffness matrix and hence the total structural stiffness was obtained in a manner similar to that described in the finite element discussion of the previous section. The nodal force vector, R, in Equation (47), consisted of known forces (in the Y-direction) for nodes 1 through 6. The force vector, $\{F\}$, due to distributed loads, was absent as indicated in Figure 14. The computer program yielded

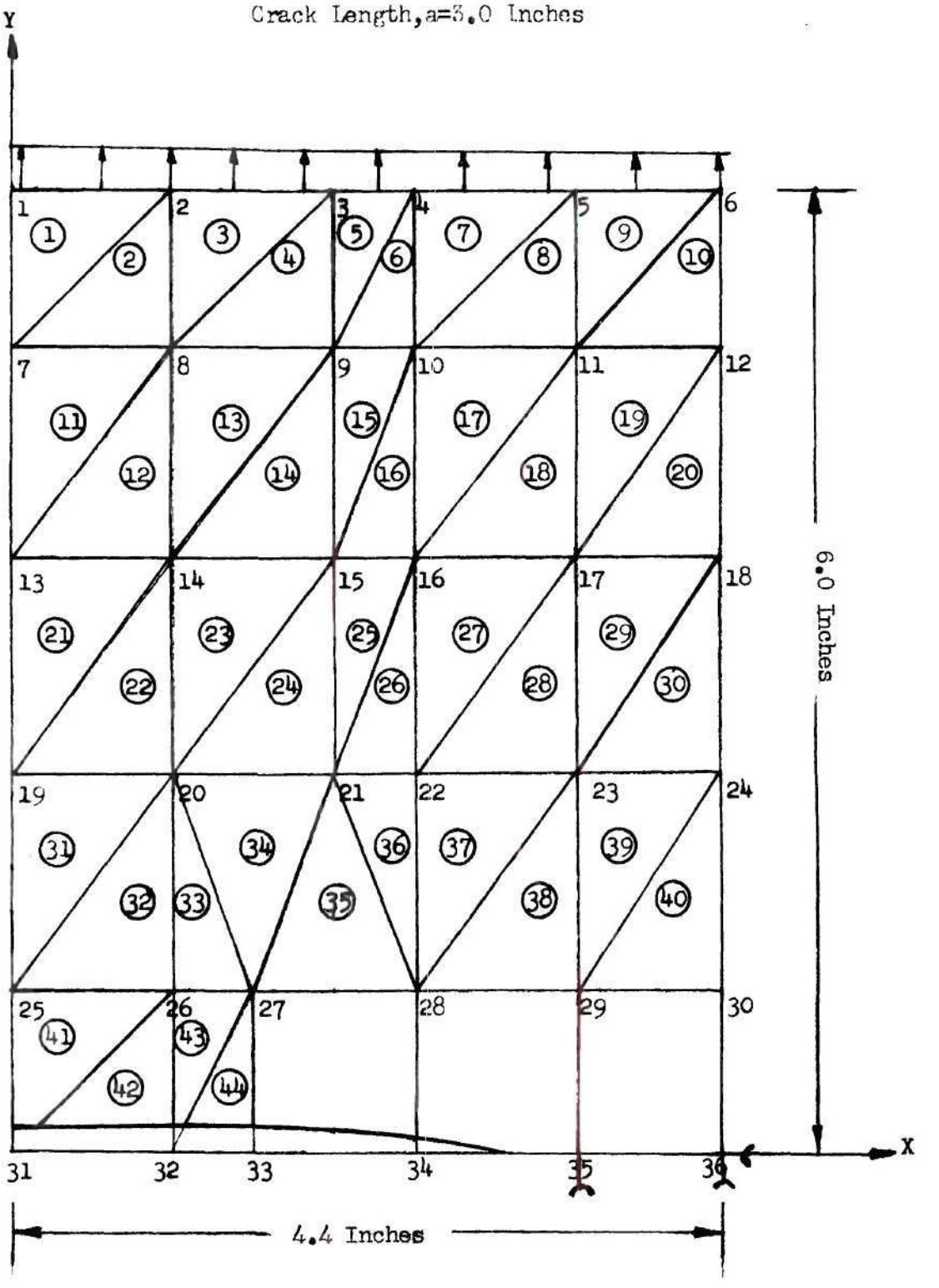

Figure 14. Finite Element Grid for Stress Distribution.

constant stresses in each triangular element and the Williams's constants for the singularity element. A program was developed to obtain the stress distribution in the special singularity element from the above obtained William's constants.

Computation of Coefficient Matrices

The matrices $[\alpha]$, $[\beta]$ and $[\Gamma]$ were required for the analysis of the free vibration, buckling, free vibration under mean load and dynamic stability problems. Only the symmetric modes were considered for these problems.

At the first stage, only the fundamental symmetric mode was used. The displacement in the lateral direction, and the rotations about the x and y axes were obtained at each node from STRUDL. Using these known quantities, the numerical values of w, and its higher order derivatives with respect to x and y, and the mixed derivatives were obtained at the center of each element in Figure 13 (see Appendix D for details).

The area integrals for the elements of the matrices as given in Appendix B were approximated by summations. For example, the elements

$$\alpha_{k\ell} = \frac{\rho h}{2g} \int\int_{\text{area}} (w_k w_\ell)\, dxdy \tag{51}$$

in terms of area integrals were replaced by the summation over the areas of the elements as follows:

$$\alpha_{k\ell} = \frac{\rho h}{2g} \sum_{i=1}^{N} w_k^{(i)} w_\ell^{(i)} A_i \tag{52}$$

where N is the total number of elements.

A_i is the area of i^{th} element in Figure 13, $w_k^{(i)}$ and $w_\ell^{(i)}$ are the lateral displacements at the center of the i^{th} element for k^{th} and ℓ^{th} modes respectively. The elements of $[\alpha]$, $[\beta]$ and $[\Gamma]$ in terms of area summations are given in Appendix E.

When considering only one mode, Equation (52) reduces to

$$\alpha_{11} = \frac{\rho h}{2g} \sum_{i=1}^{N} (w^i)^2 A_i \quad k = \ell = 1 \tag{53}$$

Similarly the matrix $[\beta]$ and $[\Gamma]$ also reduce to 1×1 matrices, and the summation expressions, when considering only one mode, are obtained by substituting k and ℓ equal to 1 in the expressions of Appendix E.

For the determination of the elements of matrix, $[\Gamma]$, we require the mean values of the stresses (σ_x, σ_y and σ_{xy}) for each of the elements which are considered in the summation. Each rectangular element in Figure 13 was divided into two triangular elements for the stress distribution analysis, except for the special cracked element. This is shown in Figure 14. In the special cracked element, the stresses at required points within the element were obtained by using the William's constants obtained from the initial stress distribution analysis. The mean value of stresses within two triangular elements in Figure 14 was used as the value of stress for rectangular element in Figure 13 within which the triangular elements were lying.

Using the constant values of initial stresses within each rectangular element, the numerical values of w and its derivatives at the center of each of these elements, and the areas of the elements, the required multiplication of various terms was carried out for each element. The

elements of the matrices $[\alpha]$, $[\beta]$ and $[\Gamma]$ were obtained for the entire plate by summing over all the elements. The final forms of these matrices are given in Appendix F.

The accuracy of the computations was evaluated for both deflection and stress functions. In the previous section, the free vibration solution using finite elements was evaluated by increasing the number of elements until satisfactory convergence was obtained.

A study of convergence in the initial stress distribution included computations for the finite element pattern of Figure 14, and subsequently led to the final use of the element pattern shown in Figure 15. Since the stress distribution was fairly uniform for the first 20 triangular elements in Figure 14, they were left undivided in Figure 15. The next 24 triangular elements (21 through 44 in Figure 14) were subdivided in such a way that four triangular elements were lying within each rectangular element of Figure 13. The special cracked element was treated as before. Adopting the same procedure as for the coarse grid, the elements of the matrices $[\alpha]$, $[\beta]$ and $[\Gamma]$ were obtained, and are presented in Appendix F. The other crack lengths were treated the same way.

At the second computational stage, the first two symmetric modes were combined. For this case the matrices $[\alpha]$, $[\beta]$ and $[\Gamma]$ are all of second order. For example, Equation (52) for element α_{12} can be written as

$$\alpha_{12} = \frac{\rho h}{2g} \sum_{i=1}^{N} w_1^{(i)} w_2^{(i)} A_i \qquad (54)$$

where 1 and 2 correspond to the mode shapes. Similarly, the remaining

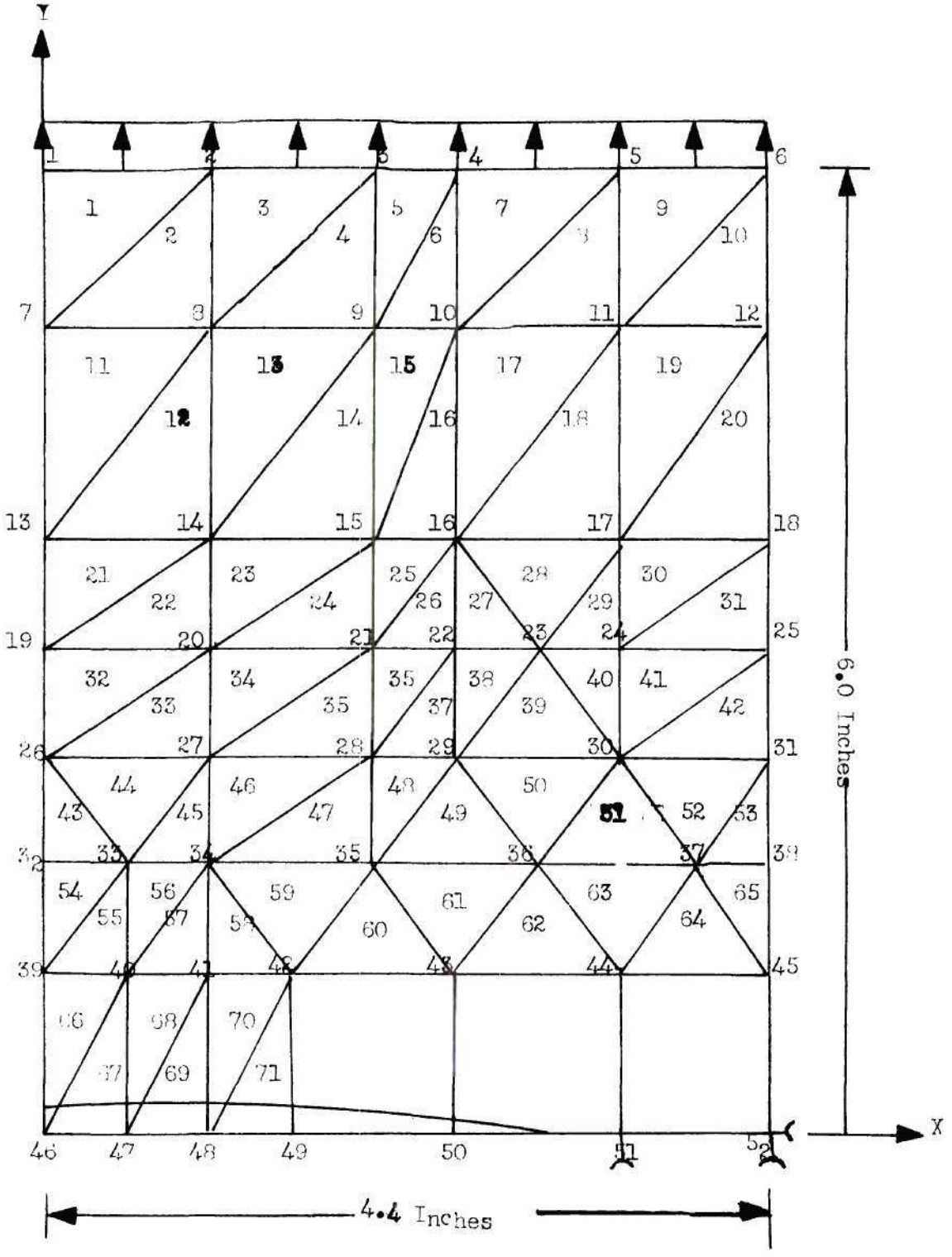

Figure 15. Refined Finite Element Grid for Stress Distribution.

elements of $[\alpha]$, and the elements of $[\beta]$ and $[\Gamma]$ can be represented by the summation expressions. Repeating the same procedure as for one mode, the elements of the matrices were obtained for a combination of the two modes. Both the coarse and refined grids for the initial stress distribution were considered. The final forms of these 2×2 energy matrices are presented in Appendix G.

The above matrices were computed for aluminum alloy 2024-T3, with material properties and dimensions as follows:

Half length of the specimen, ℓ = 6.0 inches

Width of specimen, (a+b) = 4.4 inches

Modulus of elasticity, $E = 10.6 \times 10^6$ lbs/in^2

Modulus of rigidity, $G = 4 \times 10^6$ lbs/in^2

Mass per unit volume, ρ = 0.1 lbs/in^3

Thickness of specimen, h = 0.025 inch.

The cracks lengths, a, used were 2.0, 2.5, 3.0 and 3.5 inches.

Analyses of the Problems

Each of the problems of interest is considered separately in the sections which follow. The numerical values of the elements of the appropriate coefficient matrices were used in the problems.

Free Vibration

The solution of the free vibration problem by the use of STRUDL was described previously in this chapter. The results were presented in Table 6. It should be noted, however, that the solution of the free vibration problem by the assumed mode method was also outlined in Chapter II. This method led to the development of the so-called coefficient

matrices. For the free vibration problem, these were the matrices designated as $\underline{\alpha}$ and $\underline{\beta}$. As a check on the use of STRUDL to generate the "assumed modes" required, the first mode from the STRUDL output was used as an assumed mode. The resulting coefficient matrices obtained in the previous section and listed in Appendix F, were then used to compute an associated eigenvalue from the characteristic equation

$$|\alpha - \omega^2 \beta| = 0$$

The eigenvalues, ω, are the free vibration frequencies of the system. The above equation was solved and the resultant free vibration frequencies for different crack lengths are listed in Table 7.

Table 7. Free Vibration Frequencies as Obtained by Using the Fundamental Symmetric Mode from STRUDL

a/(a+b)	Fundamental, symmetric, free vibration frequency (Hz)	
	Coarse grid	Fine grid
0.4545	34.61	34.91
0.5681	32.65	33.21
0.6818	31.29	31.85
0.7954	30.75	30.77

The respective results in Tables 6 and 7 are quite compatible and hence the modes generated were used in the analysis of the other problems.

Buckling

The determination of the static buckling load is based on Equation

(39). The characteristic determinant is given by

$$|\underline{\beta} - c\,\underline{\Gamma}| = \underset{\sim}{0} \tag{55}$$

Since the first two modes of free vibration were combined for this problem, the matrices $\underline{\beta}$ and $\underline{\Gamma}$ were of second order. Positive values of the local buckling load (tension) were expected only for crack lengths more than half the width of the plate. The computed values of the buckling loads, however, were all negative, which indicated compressive buckling loads. They are given in Table 8. The normalized eigenvectors of Equation (39), which indicate the ratios in which the two modes were combined, are also presented in Table 8.

Table 8. Computed Values of Buckling Loads and Eigenvectors

a/(a+b)	Buckling Loads (in pounds), using fine grid	Corresponding Normalized Eigenvectors
*0.0	-19.46	--
0.4545	-15.65	1.0, .0584
0.5681	-13.50	1.0, 0.0138
0.6818	-12.12	1.0, 0.0527
0.7954	-11.88	1.0, 0.0372

*The buckling load for zero crack length was obtained by using the Raleigh-Ritz method, considering only a fundamental symmetric mode.

Dynamic Stability

Here, the object is to determine the boundaries defining a transition from a stable to an unstable dynamic response in terms of mean load,

P_o, cyclic load, P_1, and the excitation frequency, λ. The governing differential Equation (37) can be rewritten as follows:

$$\underline{\alpha}\,\ddot{\underset{\sim}{f}} + [\underline{\beta} + (c + d\eta)\underline{\Gamma}]\,\underset{\sim}{f} = \underset{\sim}{0} \tag{56}$$

where $\eta(t) = \cos \lambda t$.

For this problem, only the fundamental symmetric free vibration mode shape was used to obtain the coefficient matrices $\underline{\alpha}$, $\underline{\beta}$ and $\underline{\Gamma}$. These coefficient matrices were of the first order with one constant element. A presentation of these matrices is made in Appendix F, referring to the fine grid.

If the function $\eta(t)$ is a periodic function with period T, the regions of unboundedly increasing solutions to Equation (56) above are separated from the regions of stability by the periodic solutions with periods T and 2T [5]. It is found that two solutions with identical periods bound the regions of instability and two solutions of different periods bound the regions of stability. The determination of the boundaries of the regions of instability reduces to finding the conditions (in terms of P_o, P_1 and λ) under which the governing equation, (56), has periodic solutions with periods T and 2T.

Since $\eta(t) = \cos \lambda t$ is a periodic function of period $\frac{2\pi}{\lambda}$, interest lies in finding solutions of Equation (56) which are periodic with periods $\frac{2\pi}{\lambda}$ and $\frac{4\pi}{\lambda}$, respectively. To obtain solutions with period $\frac{4\pi}{\lambda}$, substitute the fourier series,

$$\underset{\sim}{f}(t) = \sum_{k=1,3,5}^{\infty} \left[\underline{a}_k \sin \frac{k\lambda t}{2} + \underline{b}_k \cos \frac{k\lambda}{2} t\right] \tag{57}$$

in Equation (56) and reduce the result to a sum of linearly independent trigonometric functions. Since the sum is zero, two systems of homogenous matrix equations are obtained when the coefficients of the trigonometric functions are required to be zero. Applying the condition for the existence of a nontrivial solution (which is the vanishing of the determinant of the matrix), the two systems combined under the ± sign take the form:

$$\begin{vmatrix} \underline{\beta} + (c \pm \frac{1}{2} d)\underline{\Gamma} - \frac{1}{2}\lambda^2\underline{\alpha} & \frac{1}{2} d\underline{\Gamma} & 0 \\ \frac{1}{2} d\underline{\Gamma} & \underline{\beta} + c\underline{\Gamma} - \frac{9}{4}\lambda^2\underline{\alpha} & \frac{1}{2} d\underline{\Gamma} \\ 0 & \frac{1}{2} d\underline{\Gamma} & \underline{\beta} + c\underline{\Gamma} - \frac{25}{4}\lambda^2\underline{\alpha} \end{vmatrix} = 0 \qquad (58)$$

Note that the underlined terms are square matrices.

As a first approximation, only the first diagonal element of the above matrix was considered and solved to give the upper and lower boundaries of the principal region of dynamic stability.

Similarly, the equations for determining the existence of solutions to the governing equations with period $2\pi/\lambda$ are obtained by substituting the Fourier series

$$\underset{\sim}{f}(t) = \sum_{k=2,4,6}^{\infty} [\underline{a}_k \sin \frac{k\lambda t}{2} + \underline{b}_k \cos \frac{k\lambda t}{2}]$$

into Equations (56) and setting the coefficients of the linearly independent functions equal to zero. The matrix forms of these equations are as follows:

$$\begin{vmatrix} \underline{\beta} + c\underline{\Gamma} - \lambda^2\underline{\alpha} & + \frac{1}{2} d\underline{\Gamma} & \underline{0} \\ + \frac{1}{2} d\underline{\Gamma} & \underline{\beta} + c\underline{\Gamma} - 4\lambda^2\underline{\alpha} & + \frac{1}{2} d\underline{\Gamma} \\ \underline{0} & + \frac{1}{2} d\underline{\Gamma} & \underline{\beta} + c\underline{\Gamma} - 9\lambda^2\underline{\alpha} \end{vmatrix} = 0 \qquad (59)$$

and

$$\begin{vmatrix} \underline{\beta} + c\underline{\Gamma} & + d\underline{\Gamma} & \underline{0} & \underline{0} \\ + \frac{1}{2} d\underline{\Gamma} & \underline{\beta} + c\underline{\Gamma} - \lambda^2\underline{\alpha} & + \frac{1}{2} d\underline{\Gamma} & \underline{0} \\ \underline{0} & + \frac{1}{2} d\underline{\Gamma} & \underline{\beta} + c\underline{\Gamma} - 4\lambda^2\underline{\alpha} & + \frac{1}{2} d\underline{\Gamma} \\ \underline{0} & \underline{0} & + \frac{1}{2} d\underline{\Gamma} & \underline{\beta} + c\underline{\Gamma} - 9\lambda^2\underline{\alpha} \end{vmatrix} = 0 \qquad (60)$$

The fundamental free vibration mode was used to develop the matrices $\underline{\alpha}$, $\underline{\beta}$ and $\underline{\Gamma}$, and the Equations (59) and (60) were solved to obtain the upper and lower boundaries of the secondary regions of dynamic stability. The computed values of the frequency parameter, λ, for applied mean load, P_o equal to 25 lbs. for the boundaries of principal and secondary regions of dynamic stability are given in the following table for several values of P_1.

Table 9. Secondary-Region Boundaries

P_1 (lbs)		4	8	12	16
a (inch)	a/(a+b)	Excitation Frequency (Hz)			
0.0	0.0	56.0, 56.7	54.4, 57.0	51.6, 57.4	47.4, 57.9
2.0	0.4545	54.9, 55.6	53.0, 55.9	49.6, 56.5	44.4, 57.2
2.5	0.5681	54.6, 55.5	52.5, 55.8	48.6, 56.4	42.6, 57.2
3.0	0.6818	54.2, 55.1	51.9, 55.5	47.7, 56.1	41.2, 57.0
3.5	0.7954	52.8, 53.7	50.5, 54.1	46.3, 54.7	39.8, 55.5

Table 10. Principal-Region Boundaries

P_1 (lbs)		4	8	12	16
(inch)	a/(a+b)	Excitation Frequency (Hz)			
0.0	0.0	107.6, 118.5	102.0,123.8	95.4,128.9	91.0, 133.8
2.0	0.4545	105.1, 116.8	99.0,122.5	93.0,127.9	87.3, 133.3
2.5	0.5681	104.4, 116.8	97.9,122.6	91.6,128.5	83.8, 134.1
3.0	0.6818	103.5, 116.4	96.8,122.5	90.3,128.4	84.4, 134.1
3.5	0.7954	100.7, 113.4	94.2,119.4	87.8,125.2	82.1, 130.8

CHAPTER V

DISCUSSION OF RESULTS

Introduction

The results of an experimental investigation of the free vibration, buckling and parametric excitation behavior of a thin tensioned sheet with an edge crack were presented in Chapter III. The results for these problems investigated analytically were presented in Chapter IV. Assumed modes and Lagrange Equations were used in obtaining the analytical results. The definite integrals used in the method were obtained by replacing the integrals over the area by a summation over the finite elements. The free vibration modes were obtained by using STRUDL.

The analytical results for the problems mentioned above were obtained for two different cases. In the first case, the fundamental symmetric mode was used. In the second case, the first two symmetric modes were combined. For each case, two finite element grids were used; i.e., a coarse grid and a refined grid. The present chapter is devoted to the correlation of experimental and analytical results for free vibration, buckling and dynamic stability problems.

The Free Vibration Problem

Experiments were performed to determine the free vibration behavior of the cracked specimen and to check the applicability of the analytical results. The analytical results obtained by using assumed modes in terms of trigonometric and polynomial solutions were discarded in Chapter IV

because of poor correlation with the experimental results. The experimental results for free vibration frequencies, corresponding to several crack lengths were presented in Table 1. The corresponding results obtained analytically by using STRUDL were presented in Table 6. For the specimen with no crack the results were also obtained analytically by the use of the Rayleigh-Ritz method, and were tabulated along with STRUDL results.

The analytical and experimental results obtained for the free vibration frequency versus crack to width ratio [a/(a+b)] are plotted in Figure 16. As indicated by the curves, both the analytical and experimental values of frequency decrease as the crack length increases. When the crack is introduced, the plate element becomes less constrained, and the stiffness of the element decreases. Since the free vibration frequency is a function of the stiffness of the structure, it should decrease as the crack length is increased. Thus the expected physical behavior of the specimen is confirmed both by experimental and physical results.

As indicated in Figure 16, the frequency obtained by Raleigh-Ritz solution for sheet without any crack is higher than those obtained experimentally. This is in accordance with the expectation, because the Raleigh-Ritz method should give an upper bound for the lowest eigenvalue. Because of geometric complexity, Raleigh-Ritz solution was not used to analyze the specimens with edge cracks.

The experimental values of frequencies correlate well with the corresponding frequencies evaluated by STRUDL. A comparison reveals that the experimental curve is higher than the STRUDL curve up to a crack to

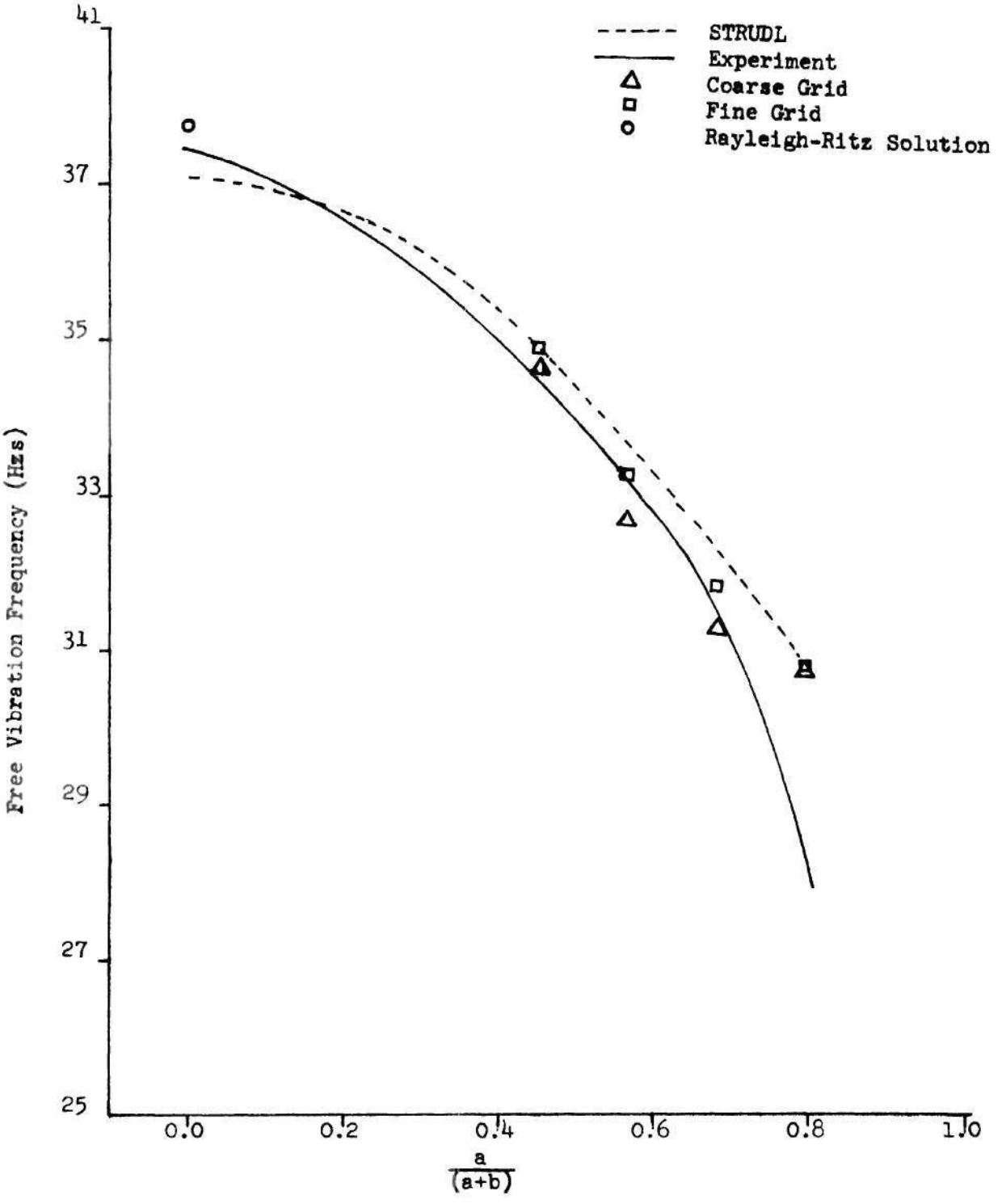

Figure 16. Free Vibration Frequencies vs. Crack to Width Ratio.

width ratio of about 0.18, and lower than the STRUDL curve for greater ratio values.

From the preceding comparison it is clear that the STRUDL results provide neither an upper nor a lower bound to the experimental frequency values. The probable reason for this may be traced to the features of the STRUDL method. First, the actual plate is replaced by a model which introduces a relaxation of internal constraints at the interfaces of the elements. That is, deflections are continuous at the element interfaces, but slopes are continuous only at nodes. A model of this type would be expected to have a smaller natural frequency than the actual plate. The computational procedure, however, provides an approximate frequency for the model. Since this approximation is equivalent to the use of a Ritz procedure, the result should be a frequency which is greater than that for the model. Thus, although the computed result is high for the model, the true model value is lower than that for actual plate. From these conditions, it would follow that the STRUDL estimates could be either greater or less than those of the actual structure.

In view of the character of the STRUDL approximation, it follows that results for different grid sizes should be obtained to evaluate the convergence behavior of the method. Although different grid sizes were used in the present investigation, extensive numerical comparisons were not conducted because of the availability of experimental results.

Since the mode shapes obtained analytically from STRUDL were to be used in the determination of the coefficient matrices required for the solution of buckling and dynamic stability problems, a check on the accuracy of their applicability was desirable. If the deflection functions

derived by STRUDL for each element were used in the assumed modes method utilizing Lagrange's Equations, the natural frequencies obtained for free vibration should be the same as those for the dashed curve of Figure 16. This would, of course, require that the necessary definite integrals be integrated over each of the elements. Since derivatives of polynomial functions are involved, this would not be difficult. For the other problems of interest, however, a complex initial stress state is present and the integrals become too complex for analytical integration.

It is common for such problems to develop an approximate numerical scheme of integration. Because of symmetry, only half the plate was considered. This was noted previously.

For the STRUDL analysis 30 rectangular elements were used. For the approximate analysis described here as the "coarse grid," 29, 38, 27 and 33 rectangular elements were used corresponding to crack lengths of 2.0, 2.5, 3.0 and 3.5 respectively. The choice of the number of rectangular elements used depended upon the number of triangular elements that were used for the nonuniform initial stress problem. An attempt was made to fit two triangular elements of the initial stress distribution grid into each rectangular element used for free vibration. The values of the required derivatives of the deflection function were taken as constant for each element. These constant values were determined at the centre of each rectangular element by making use of the known values of lateral displacement and angular rotations about x and y axes at each of the four nodes of the element. These known values were obtained from the STRUDL output, and a complete procedure used in determining the deflection function and its derivatives is outlined in Appendix D. The definite

integrals were approximated by appropriately summing the results for all of the elements multiplied by the areas of the individual elements. The free vibration results of these analyses were presented in Table 7, and are plotted as open triangular data points in Figure 16.

To determine the effect of the size of the elements used, a second series of computations were performed. For these, 47, 53, 53 and 61 rectangular subelements were used for crack lengths of 2.0, 2.5, 3.0 and 3.5, respectively. The constant values of deflection function and its derivatives at the centre of each of these sub-elements were obtained from the known information at the nodes of STRUDL elements as before. The results of these analyses and so called "fine grid" analyses were presented in Table 7. They are plotted in Figure 16, as open square data points.

A comparison of the results indicates that for each case the fine grid results are closer to the STRUDL curve. This is the proper trend and since the correlation is acceptable, the outlined numerical scheme was adopted for subsequent problems. The fine grid was used for all computations.

The Dynamic Stability Problem

The dynamic stability behavior of the tensioned sheet with an edge crack was studied both experimentally and analytically. The analytical results for boundaries of secondary and principal regions of dynamic instability were obtained in Chapter IV. They were presented in Tables 9 and 10. For each crack length these results were obtained for a mean load of 25 lbs., and alternating loads of 4, 8, 12 and 16 lbs. Several

crack lengths were considered. For the uncracked plate, the analysis was carried out by using direct Raleigh-Ritz method and by considering the fundamental symmetric mode only. For the cracked plate, the results were obtained by using the fundamental symmetric mode from STRUDL. A good correlation of results for free vibration behavior were obtained by using this mode (see Figure 16), and the associated mode should have approximately the right shape for the dynamic stability problem. Naturally, improved results could be expected if additional symmetric modes were used. The computational work increases rapidly, however, for more modes.

The experimental results were presented in Table 2. The purpose of this section is to correlate the analytical and experimental results. The effects of edge crack length on the dynamic stability are particularly emphasized. The behavior of lateral deflections of plate during oscillations is also studied.

Regions of dynamic instability are often effectively described in terms of dimensionless ratios involving the frequency and load parameters. The ratios are developed with reference to the static buckling load and the natural frequency of free vibrations with initial load. Since the use of these parameters does not add to an understanding of the results obtained, however, the results obtained in the previous chapters by analytical and experimental means will be discussed here in terms of the measured quantities.

The data of Tables 2, 9 and 10 are presented in Figures 18 and 19, as plots of excitation frequency versus the alternating load, P_1. The plots are made for crack lengths of 0.0, 2.0, 2.5 and 3.0 inches. The experimental results for crack lengths of 2.5 and 3.0 inches were obtained

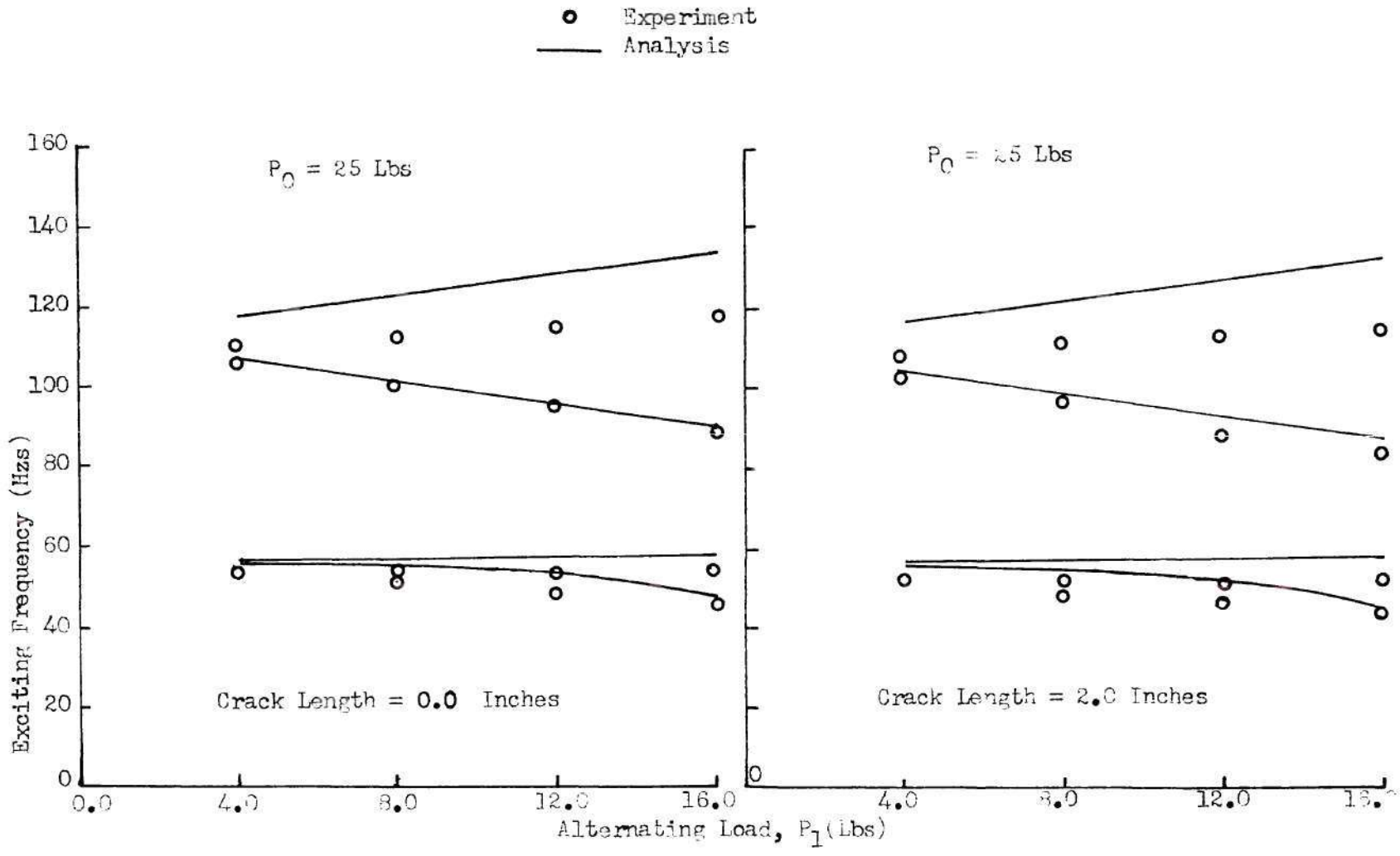

Figure 17. Dynamic Stability Plots.

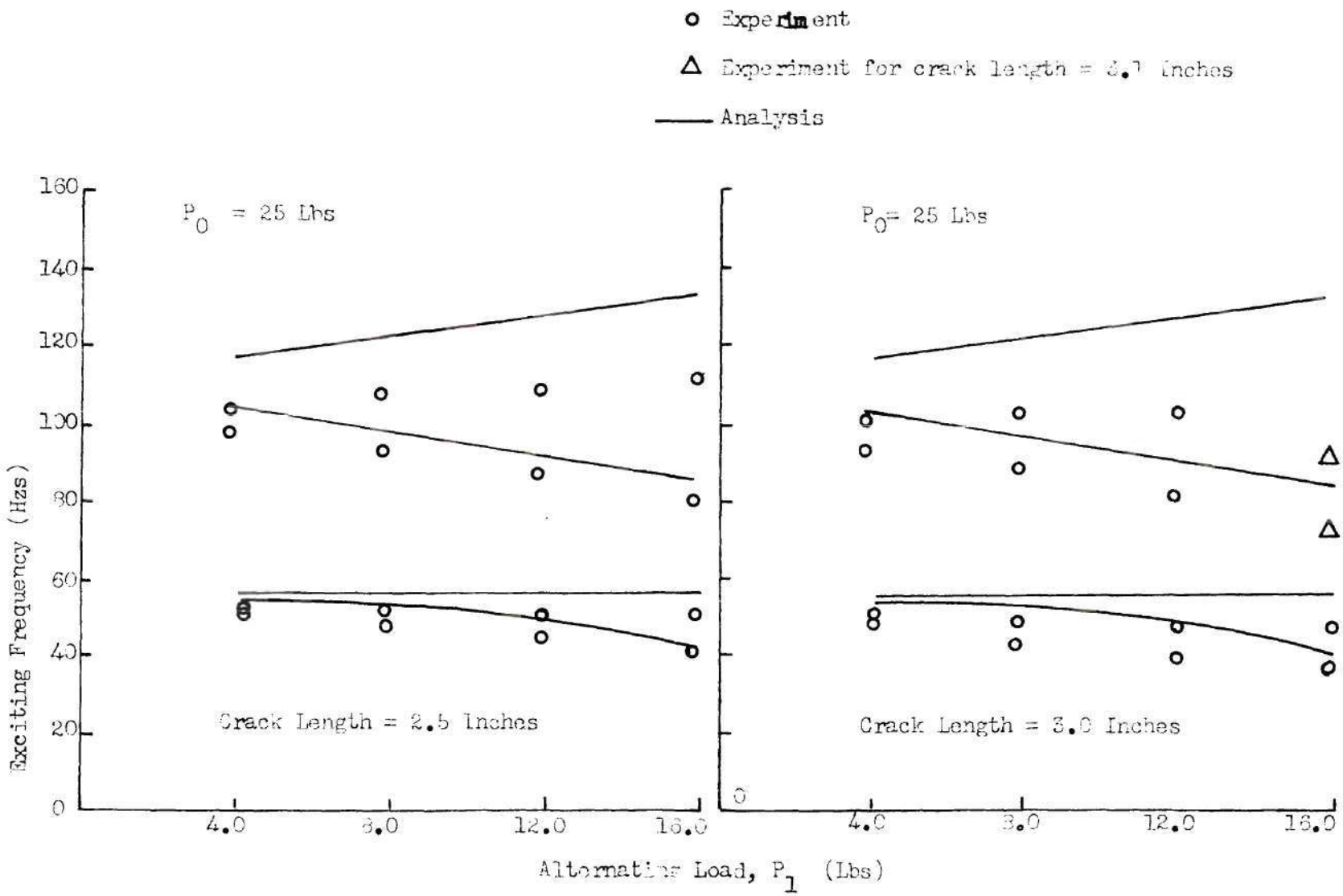

Figure 18. Dynamic Stability Plots.

from data of Table 2 by interpolation.

An insight into the curves of Figures 17 and 18, reveals that the size of the principal regions is substantially larger than the secondary regions. It is also clear that as the value of P_1 increases, the range of excitation frequencies within which the principal and secondary regions of instability are developed, increases. This behavior is exhibited by both the analytical and experimental curves.

A comparison of analytical and experimental plots of Figure 17 and 18 shows that the boundaries of instability regions obtained analytically are higher than the corresponding boundaries obtained experimentally. It can also be observed that the sizes of instability regions obtained analytically are slightly larger than the sizes of the same regions plotted from experimental results. Both of these observations lead to conjecture about sources of the observed differences.

It has been noted previously that the analysis is approximate. Among possible sources for error attributable to the analysis are:

1. The approximation features of the finite element analysis.

2. The numerical integrations performed to compute the definite integrals.

3. The use of only one mode to represent the dynamic stability behavior.

4. The neglect of damping, middle surface stretching and inplane inertia effects.

Some attention should also be directed to the experimental results. Since the analytical results are always above the experimental results, it would appear possible a consistent source of error. A simple possibility

which could, if corrected, substantially improve the correlation is a difference in the specimen and analytical model length. The latter length used is the measured length of the former. Due to the impossibility of achieving clamped edges, however, the experimental effective length may be greater than the measured length. This could account for the consistent directional difference observed.

If the analytical plots for values of P_1 were continued below 4 pounds, the curves for the upper and lower boundaries of principal regions would meet at P_1 equal to zero pounds. The same is true for secondary regions. It indicates that, theoretically, instability occurs for all nonzero values of P_1. If we perform an extrapolation for experimental plots to P_1 less than 4 pounds, the curves corresponding to the upper and lower boundaries of unstable regions meet at positive values of P_1 larger than zero. This means that there are minimum values of P_1 below which instability does not occur. This difference between analytical and experimental results is due to the effect of damping. In the analysis of dynamic stability, the effect of damping was ignored. But in the experimental investigation of dynamic stability this effect is present.

The effect of crack length on dynamic stability is described by the plots of Figures 17 and 18. As the crack length increases, boundaries of the instability regions become lower. This is true for the experimental, as well as, analytical results. Also, the extrapolation of the experimental curves similar to the one performed in the preceding paragraph indicates that as the crack length is increased, the minimum value of P_1, below which the instability does not occur, is decreased. Both

of these effects are in accordance with our expectation. They are directly functions of specimen stiffness, and the stiffness decreases as the crack length is increased. The overall effect is dynamically destabilizing.

Another aspect of the destabilizing effect may be developed by considering the nondimensionalized areas of the instability regions. The areas of the principal and secondary regions of instability were computed for various crack lengths for both experimental and analytical results. The total areas; i.e., the sum of the principal and secondary regions for these crack lengths were nondimensionalized with respect to the total area at a crack length of zero. A plot of these dimensionless areas versus the crack to width ratio is shown in Figure 19. As indicated by the analytical and experimental curves, the effect of increasing the crack length is dynamically destabilizing. This confirms the expected behavior.

A comparison of analytical and experimental curves of Figure 19, indicates that the correlation between the two is fairly good. The analytical values of dimensionless instability areas appear, therefore, to provide an acceptable representation of the change in the instability zones with increasing crack length.

A discussion of the effect of crack length on the transverse deflections, is also of interest. Experimental data were obtained for each crack length for a mean tensile load of 25 pounds and an alternating load of 16 pounds. The transverse deflections were measured for principal and secondary regions of instability at the outer edge of the crack (point A of Figure 9). The data obtained were presented in Table 3. Plots of

A = Total Area of Principal and Secondary Regions of Instability.

A_0 = Total Area of Principal and Secondary Regions of Instability for Crack Length Equal to Zero.

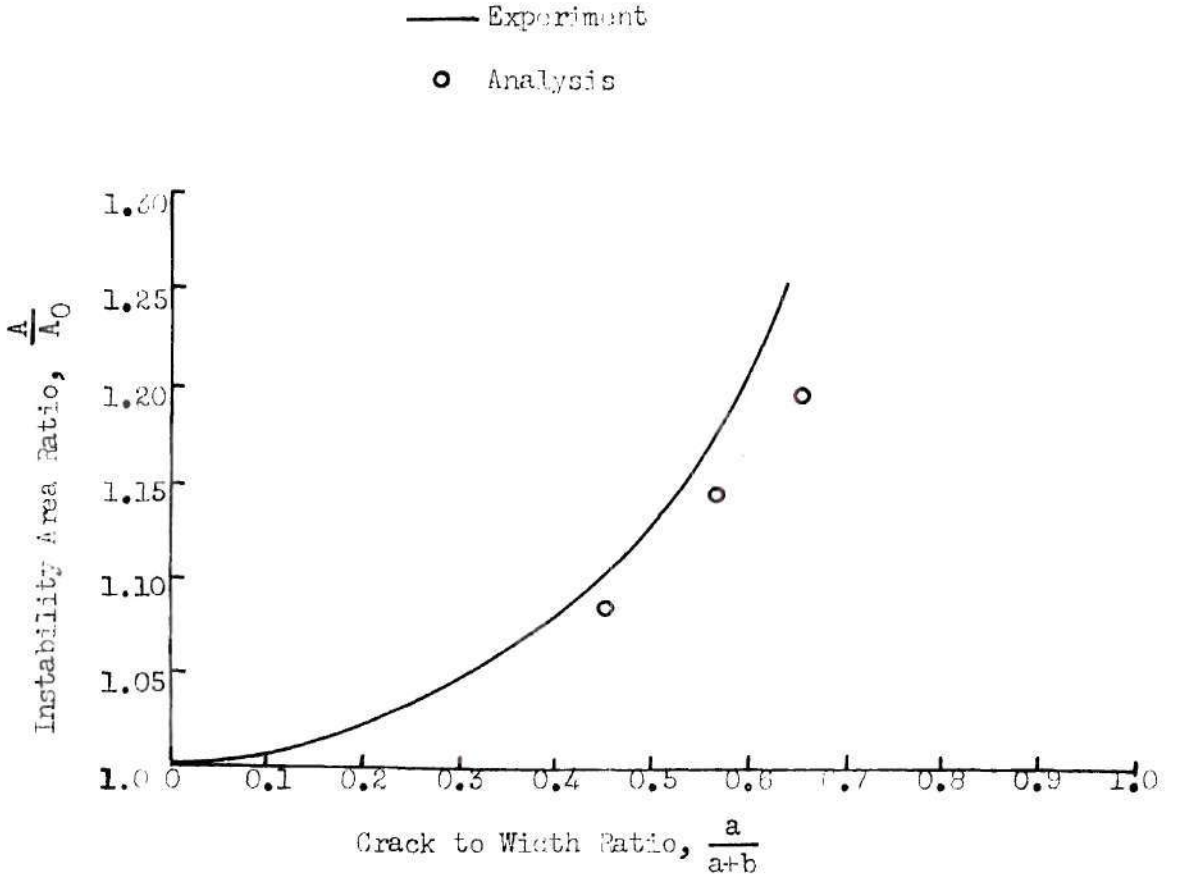

Figure 19. Dynamic Instability Area Plots.

lateral deflections versus crack to width ratio are shown in Figure 20. For oscillations within the principal regions the transverse deflections increased from ten times to about twenty times the thickness of the sheet as the crack length increased from zero to 3 inches. Under the same conditions, and for oscillations within the secondary regions, the deflections doubled from five to ten times the thickness of the sheet.

The nonlinear effect of mid-surface stretching due to bending for the large deflections is of interest. This is a stiffening effect and it results in the overhang behavior which led to the adoption of the experimental procedure described in Chapter III.

Another interesting aspect of large deflections is associated with its effect on the propagation of the crack. These large amplitude oscillations combined with mean tension may be expected to effect the propagation of crack significantly. As the crack length increases, the stress intensity factors at the crack tip and the amplitude of transverse deflections also increase. These two factors did, in fact, cause the crack to propagate when the sheet was oscillating within the principal regions for crack lengths of 2.8 and 3.1 inches.

Buckling Problem

As mentioned before, the possibility of local buckling in the region adjacent to the tip of the crack is of interest. This tensile local buckling would be expected to be possible only for cracks exceeding a certain critical length.

Experiments were conducted to determine the tensile buckling loads

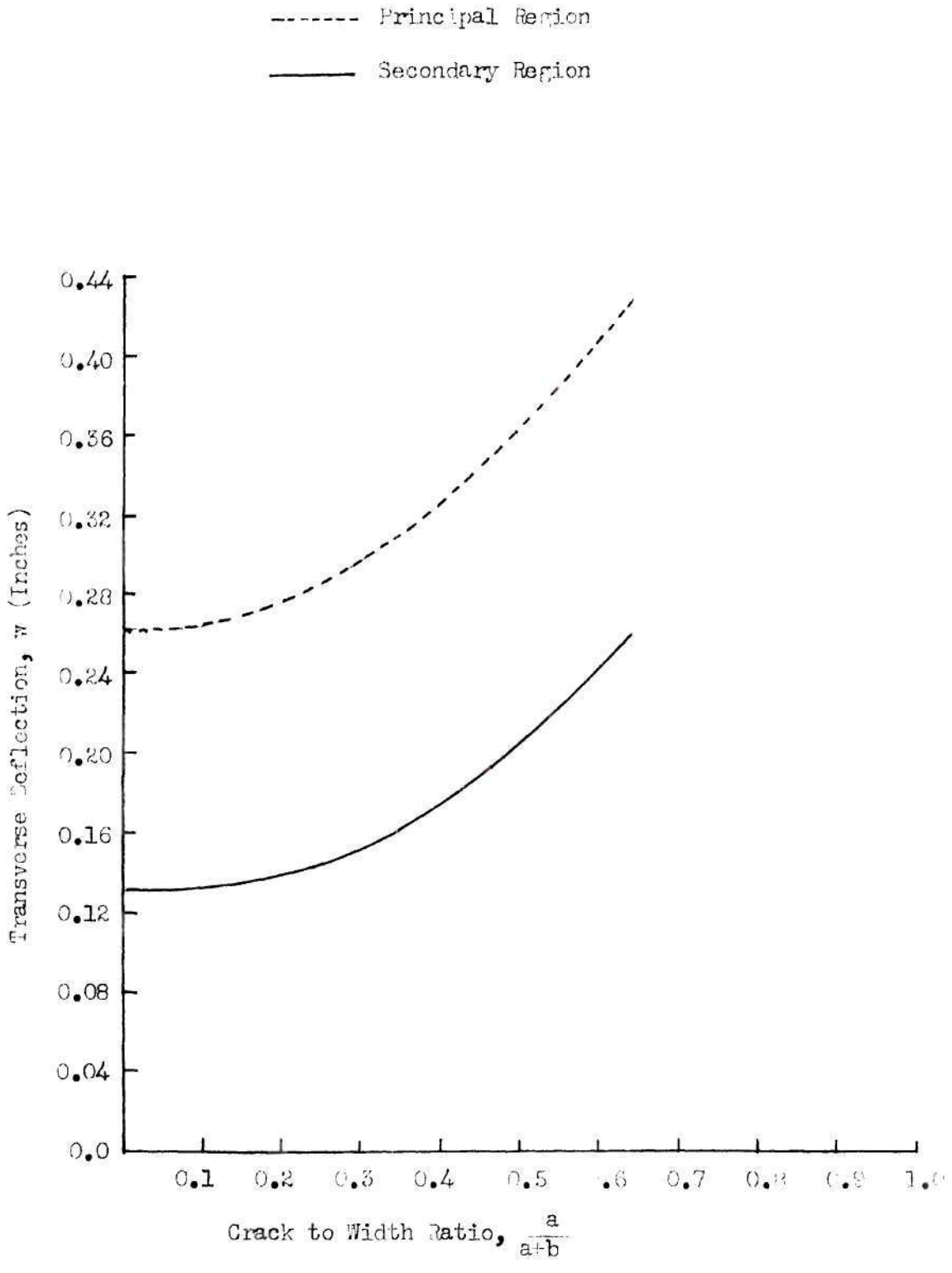

Figure 20. Experimental Transverse Deflection Plots

for several crack lengths and the results were presented in Table 4. To represent the local buckling shape analytically, the use of more than one free vibration mode shapes would be expected to be necessary. The coefficient matrices used for the analytical determination of local buckling loads were, therefore, obtained by using the first two symmetric free vibration modes from STRUDL. The analysis was performed to determine the buckling loads and eigenvectors (the ratio in which the two modes are combined) for various crack lengths, and the results were presented in Table 7.

The negative sign of the buckling loads in Table 7 indicates that the buckling loads obtained are compressive. An examination of the eigenvectors reveals that the main contribution to the buckling load was provided by the fundamental symmetric mode. This indicates that more free vibration modes need to be used in the analysis of buckling in order to detect tensile buckling.

Since the compressive buckling loads for sheet with edge crack were not of interest, the analytical results have not been plotted. Due to the nonavailability of analytical tensile buckling loads, the experimental tensile buckling loads also have not been plotted.

CHAPTER VI

CONCLUSIONS AND RECOMMENDATIONS

Conclusions

The objective of this dissertation was to analyze and study experimentally the free vibration, local buckling and dynamic instability behavior of a tensioned sheet with an edge crack. Particular emphasis was placed on the effect of the length of the edge crack on the above described behavior. A review and correlation of the results led to conclusions which are summarized in the discussion which follows.

The free vibration problem was analyzed by using assumed modes in Lagrange's Equations. When trigonometric and polynomial functions were used, a poor correlation with experimental results was obtained.

The free vibration frequencies and mode shapes were also obtained by using STRUDL which makes use of the finite element method. In STRUDL no attempt was made to consider the effect of the stress singularity at the tip of the crack. The frequencies obtained had fairly good correlation with the experimental frequencies.

As an alternative solution to the problem of interest, the free vibration modes generated by STRUDL were used as assumed modes in Lagrange Equations. An approximate numerical integration scheme was developed and the results for two different mesh sizes were obtained. Agreement with both the experimental results and STRUDL results was good for the finer mesh. The numerical integration scheme was used as a basis for analyzing the buckling and dynamic stability problems.

The finite element method was used to determine the non-uniform stress distribution throughout the tensioned sheet with an edge crack. The stress singularity at the crack tip was taken care of by using a singularity element for the symmetric case. This stress distribution and the partial derivatives obtained from STRUDL output were used in evaluating the external potential.

The first two symmetric modes obtained from STRUDL were used in constructing the second order coefficient matrices for the internal and external potentials. These coefficient matrices were used in analyzing the tensile local buckling loads. Only compressive buckling loads were obtained. This indicated that two modes were not sufficient to represent both the global (compressive) and local (tensile) buckling behavior.

The coefficient matrices obtained by using the fundamental free vibration mode from STRUDL were used to determine, analytically, the principal and secondary regions of dynamic stability. The analytical regions of instability were larger than those obtained experimentally, and they were located at higher levels of excitation frequencies. The correlation was, however, good enough to be of engineering value in approximately predicting the dynamic stability behavior.

The effect of edge crack length on free vibration and dynamic stability was studied. The free vibration frequency decreased by about 20 percent as the crack to width ratio increased from zero to 0.8. For dynamic stability the principal and secondary regions of instability grew in size and were located at lower values of excitation frequencies as the crack length increased. The total size of instability regions increased by about 1.25 times as the crack to width ratio increased from

zero to about 0.65. For these effects a good correlation between the analytical and experimental results was observed.

The crack propagated during oscillations of the specimen within the principal region of dynamic instability when an experiment was being conducted at a mean load of 25 pounds, an alternating load of 16 pounds, and a crack length of 2.8 inches. Under the same conditions and at a crack length of 3.1 inches, the crack propagation was again observed. Clearly, these conditions were critical for the specimen.

The transverse deflections were measured for a mean load of 25 pounds, and an alternating load of 16 pounds. For oscillations within principal regions, the deflections increased from about ten to twenty times the thickness of the plate as the crack length increased from zero to about three inches. For a similar increase in crack length, the deflections within secondary regions were observed to increase from about five to ten times the sheet thickness. This type of resonant behavior could be expected to lead to severe fatigue crack propagation problems.

Recommendations

In the course of the investigation described herein several features concerning the free vibration, local tensile buckling and dynamic stability behavior of tensioned sheet with an edge crack were observed. A more thorough understanding of these features could be attained through extensions of the present work. Recommendations for future research in these areas are suggested in the following discussion.

1. In the formulation of the Governing Differential Equation, the Gaussian curvature was assumed to be small which led to the neglect of

mid-surface stretching due to bending. For the large lateral deflections observed during the experimental investigation, these curvatures are not small. This suggests that the mid-surface stretching, which is a non-linear effect, should be considered.

2. During the analytical investigations, damping was not considered. Since the presence of damping is inevitable, its contribution should be included in an analysis.

3. The tensile buckling loads could not be determined analytically by the use of first two symmetric modes from STRUDL. A proper combination of more than two suitable modes obtained for free vibration from STRUDL should be made to analyze the problem. An alternate method might also be to represent the local buckling mode by some appropriate polynomial or trigonometric function.

4. The correlation between the analytical and experimental results for dynamic stability problem was fairly good with the use of only the fundamental free vibration mode. The analytical results may be improved by using more than one of the free vibration modes.

5. The difficulty in achieving clamped edges possibly led to an effective length which was larger than the measured length. This discrepancy might be eliminated by redesigning and improving the method of clamping the edges. Another alternative would be to develop a method for experimentally deducing the effective length of the specimen.

6. In the analysis of the dynamic stability and buckling problems the finite element method was used separately for the free vibration problem (STRUDL) and then for the non-uniform stress distribution. The results of the two problems were then combined to analyze the dynamic

stability and buckling problems. In both of the finite element analyses the basic data inputs were very similar. Moreover, coefficient matrices were developed in both finite element programs. They were then introduced into the analyses of the free vibration in the STRUDL and the initial stress distribution. The similar coefficient matrices were then developed once again, and were used in the analyses of the dynamic stability and tensile buckling problems. By way of simplification, one finite element program which can take care of all three basic problems should be developed; i.e., the free vibration, tensile buckling and dynamic stability problems. This approach would reduce both programming time and computer time.

APPENDIX A

SOME USEFUL RELATIONS

In the relations which follow summation convention is used; i.e., repeated indices indicate summation. Also, a subscript comma followed by x or y represents differentiation with respect to the indicated variable. A dot over f_k indicates differentiation with respect to time.

$$\bar{w}(x,y,t) = f_k(t)w_k(x,y)$$

$$\dot{\bar{w}} = \dot{f}_k w_k$$

$$(\dot{w})^2 = \dot{f}_k \dot{f}_\ell \, w_k w_\ell$$

$$\left(\frac{\partial \bar{w}}{\partial x}\right) = f_k w_{k,x}$$

$$\left(\frac{\partial \bar{w}}{\partial y}\right) = f_k w_{k,y}$$

$$\left(\frac{\partial^2 \bar{w}}{\partial x \partial y}\right) = f_k w_{k,xy}$$

$$\left(\frac{\partial^2 \bar{w}}{\partial x^2}\right) = f_k w_{k,xx}$$

$$\left(\frac{\partial^2 \bar{w}}{\partial y^2}\right) = f_k w_{k,yy}$$

$$\left(\frac{\partial \bar{w}}{\partial x}\right)^2 = f_k f_\ell w_{k,x} w_{\ell,x}$$

$$\left(\frac{\partial \bar{w}}{\partial y}\right)^2 = f_k f_\ell \, w_{k,y} w_{\ell,y}$$

$$\left(\frac{\partial^2 \bar{w}}{\partial x \partial y}\right)^2 = f_k f_\ell \, w_{k,xy} w_{\ell,xy}$$

$$\left(\frac{\partial^2 \bar{w}}{\partial x^2} \cdot \frac{\partial^2 \bar{w}}{\partial y^2}\right) = f_k f_\ell \, w_{k,xx} w_{\ell,yy}$$

$$\left(\frac{\partial^2 \bar{w}}{\partial x^2} + \frac{\partial^2 \bar{w}}{\partial y^2}\right)^2 = [f_k f_\ell \, w_{k,xx} w_{\ell,xx} + f_k f_\ell \, w_{k,yy} w_{\ell,yy}$$

$$+ 2 f_k f_\ell \, w_{k,xx} w_{\ell,yy}]$$

APPENDIX B

MATRIX ELEMENTS

The matrix elements referred to in Chapter II are as follows:

$$\alpha_{k\ell} = \frac{\rho h}{2g} \int\int_{\text{area}} (w_k w_\ell) dxdy$$

$$\beta_{k\ell} = \beta_{k\ell}^{(1)} + \beta_{k\ell}^{(2)} + \beta_{k\ell}^{(3)} + \beta_{k\ell}^{(4)} + \beta_{k\ell}^{(5)}$$

$$\beta_{k\ell}^{(1)} = \frac{D}{2} \int\int_{\text{area}} (w_{k,xx} w_{\ell,xx}) dxdy$$

$$\beta_{k\ell}^{(2)} = \frac{D}{2} \int\int_{\text{area}} (w_{k,yy} w_{\ell,yy}) dxdy$$

$$\beta_{k\ell}^{(3)} = D \int\int_{\text{area}} (w_{k,xx} w_{\ell,yy}) dxdy$$

$$\beta_{k\ell}^{(4)} = -1(1 - v) D \int\int_{\text{area}} (w_{k,xx} w_{\ell,yy}) dxdy$$

$$\beta_{k\ell}^{(5)} = (1-v)\, D \int\int_{\text{area}} (w_{k,xy} w_{\ell,xy}) dxdy$$

$\beta_{k\ell}^{(3)}$ and $B_{k\ell}^{(4)}$ can be combined to give

$$\beta_{k\ell}^{(6)} = Dv \int\int_{\text{area}} (w_{k,xx} w_{\ell,yy}) dxdy$$

finally:

$$\beta_{\gamma s} = \beta_{k\ell}^{(1)} + \beta_{k\ell}^{(2)} + \beta_{k\ell}^{(5)} + \beta_{k\ell}^{(6)}$$

$$\gamma_{k\ell} = \gamma_{k\ell}^{(1)} + \gamma_{k\ell}^{(2)} + \gamma_{k\ell}^{(3)}$$

where

$$\gamma_{k\ell}^{(1)} = \frac{1}{2} \int\int_{\text{area}} \bar{N}_x (w_{k,x} w_{\ell,x}) dxdy$$

$$\gamma_{k\ell}^{(2)} = \frac{1}{2} \int\int_{\text{area}} \bar{N}_y (w_{k,y} w_{\ell,y}) dxdy$$

$$\gamma_{k\ell}^{(3)} = \int\int_{\text{area}} \bar{N}_{xy} (w_{k,x} w_{\ell,y}) dxdy$$

APPENDIX C

IN-PLANE FORCE PARAMETERS

The in-plane forces per unit length ($\bar{N}_x$, $\bar{N}_y$ and $\bar{N}_{xy}$), from Equation (25) may be written as

$$\bar{N}_i = N_i + \bar{N}_{it} \cos \lambda t \quad \text{where } i = x,y$$

or

$$\bar{N}_i = c\ p_i(x,y) + d\ p_{it}(x,y) \cos \lambda t$$

where c and d are constants and are the force amplitude parameters in the mean and periodic components of the applied load.

The functions $p_i(x,y)$ and $p_{it}(x,y)$ are the in-plane forces per unit length, developed by unit magnitudes of mean and alternating loads, respectively (see loads P_o and P_1 of Figure 4). Since mean and alternating loads are both in-plane loads and produce the same spatial distributions,

$$p_i(x,y) = p_{it}(x,y),$$

It then follows that

$$\bar{N}_i = (c + d \cos \lambda t)\ p_i(x,y).$$

Also, $p_i(x,y) = h\ \sigma_i(x,y)$

where $\sigma_i(x,y)$ are the stresses developed by a unit load.

From previous work, we defined

$$\gamma_{k\ell}^{(1)} = \frac{1}{2} \int\int_{\text{area}} \bar{N}_x \, w_{k,x} w_{\ell,x} \, dxdy \, .$$

Thus

$$\gamma_{k\ell}^{(1)} = \frac{1}{2} \int\int_{\text{area}} (c + d \cos \lambda t) \, p_i(x,y) w_{k,x} w_{\ell,x} \, dxdy$$

Finally,

$$\gamma_{k\ell}^{(1)} = (c + d \cos \lambda t) \, \frac{h}{2} \int\int_{\text{area}} \sigma_x \, w_{k,x} w_{\ell,x} dxdy$$

or

$$\gamma_{k\ell}^{(1)} = (c + d \cos \lambda t) \Gamma_{k\ell}^{(1)}$$

where

$$\Gamma_{k\ell}^{(1)} = \frac{h}{2} \int\int_{\text{area}} \sigma_x w_{k,x} w_{\ell,x} \, dxdy \, .$$

Similarly

$$\gamma_{k\ell}^{(2)} = (c + d \cos \lambda t) \Gamma_{k\ell}^{(2)} \, ,$$

and

$$\gamma_{k\ell}^{(3)} = (c + d \cos \lambda t) \Gamma_{k\ell}^{(3)}$$

where

$$\Gamma_{k\ell}^{(2)} = \frac{h}{2} \int\int_{\text{area}} \sigma_y \, w_{k,y} w_{\ell,y} \, dxdy \, ,$$

and

$$\Gamma_{k\ell}^{(3)} = h \int\int_{\text{area}} \sigma_{xy} w_{k,x} w_{\ell,y} \, dxdy$$

Since

$$\Gamma_{k\ell} = \Gamma_{k\ell}^{(1)} + \Gamma_{k\ell}^{(2)} + \Gamma_{k\ell}^{(3)} ,$$

it follows that

$$\gamma_{k\ell} = (c + d \cos \lambda t)\Gamma_{k\ell} ,$$

where

$$\Gamma_{k\ell} = \Gamma_{k\ell}^{(1)} + \Gamma_{k\ell}^{(2)} + \Gamma_{k\ell}^{(3)}$$

APPENDIX D

DEVELOPMENT OF DISPLACEMENT FUNCTION FROM KNOWN NODAL DISPLACEMENTS AND ROTATIONS

The numerical values of the element displacement function and its derivative at the centre of each element are presented in this appendix. If we consider a rectangular element, ijkℓ, in Figure 13, the lateral displacements, w, and angular rotations, θ_x and θ_y, are obtained from STRUDL output at each node of the element. Knowing these twelve quantities, a displacement function for the element with twelve unknown constants can be formulated. Assume the displacement function

$$w^e = \alpha_1 + \alpha_2 x + \alpha_3 y + \alpha_4 xy + \alpha_5 x^2 + \alpha_6 y^2 + \alpha_7 xy^2 + \alpha_8 y^3 + \alpha_9 x^2 y + \alpha_{10} x^3 + \alpha_{11} xy^3 + \alpha_{12} x^3 y \qquad \text{(D-1)}$$

This can be evaluated at the nodes, i,j,k and ℓ as*

$$w_i^e = \alpha_1 + \alpha_2 x_i + \alpha_3 y_i + \alpha_4 x_i y_i + \ldots + \alpha_{12} x_i^3 y_i$$

$$w_j^e = \alpha_1 + \alpha_2 x_j + \alpha_3 y_j + \ldots + \alpha_{12} x_j^3 y_j$$

$$w_k^e = \alpha_1 + \alpha_2 x_k + \ldots + \alpha_{12} x_k^3 y_k$$

$$w_\ell^e = \alpha_1 + \alpha_2 x_\ell + \ldots + \alpha_{12} x_\ell^3 y_\ell$$

---

*Repeated subscripts do not imply summation here.

and

$$\theta_{ix} = -\frac{\partial w_i^e}{\partial y} = -\alpha_3 - \alpha_4 x_i - \qquad\qquad - \alpha_{12} x_i^3$$

etc. for j, k and ℓ.

$$\theta_{\ell y} = \frac{\partial w_\ell^e}{\partial y} = \alpha_2 + \alpha_4 y_\ell + \qquad\qquad 3\alpha_{12} x_\ell^2 y_\ell$$

etc. for j, k and ℓ.

These linear equations can be written in the matrix form as:

$$\begin{Bmatrix} w_i^e \\ \cdot \\ \cdot \\ \cdot \\ \theta_{\ell y} \end{Bmatrix} = \begin{bmatrix} 1 & x_i & \cdots & x_i^3 y_i \\ \vdots & & & \vdots \\ 0 & 1 & \cdots & 3x_\ell^2 y_\ell \end{bmatrix} \begin{Bmatrix} \alpha_1 \\ \cdot \\ \cdot \\ \cdot \\ \alpha_{12} \end{Bmatrix}$$

$$\underset{\sim}{W} = \underline{S}\ \underset{\sim}{A}$$

The unknown column matrix $\underset{\sim}{A}$ may be written as

$$\underset{\sim}{A} = S^{-1}\ \underset{\sim}{W}$$

where the 12×12 matrix $\underline{S}^{-1}$ is the inverse of $\underline{S}$.

Computation of the matrix $\underset{\sim}{A}$ gives the numerical values of twelve constants in Equation (D-1), for each element. The function, w, its first and second partial derivatives with respect to x and y, and the mixed derivatives can, then, be determined at the centre of each element. Knowing these derivatives and the in-plane stress distribution, the numerical values of the elements of the coefficient matrices $\underline{\alpha}$, $\underline{\beta}$ and $\underline{\Gamma}$ can be obtained.

APPENDIX E

MATRIX ELEMENTS AS SUMMATIONS

The elements of matrices $\underline{\alpha}$, $\underline{\beta}$ and $\underline{\Gamma}$ represented area integrals in Appendices B and C. In this appendix the definite integrals are replaced by the summations. These elements are referred to in Chapter IV, where i denotes the i^{th} element, N denotes the total number of elements, and A_i is the area of the i^{th} element

$$\alpha_{k\ell} = \frac{\rho h}{2g}\left[\sum_{i=1}^{N}(w_k^{(i)}w_\ell^{(i)})A_i\right]$$

$$\beta_{k\ell} = \beta_{k\ell}^{(1)} + \beta_{k\ell}^{(2)} + \beta_{k\ell}^{(5)} + \beta_{k\ell}^{(6)}$$

where

$$\beta_{k\ell}^{(1)} = \frac{D}{2}\left[\sum_{i=1}^{N} w_{k,xx}^{(1)}w_{\ell,xx}^{(i)}\ A_i\right]$$

$$\beta_{k\ell}^{(2)} = \frac{D}{2}\left[\sum_{i=1}^{N} w_{k,yy}^{(i)}w_{\ell,yy}^{(i)}\ A_i\right]$$

$$\beta_{k\ell}^{(5)} = (1-v)\ D\left[\sum_{i=1}^{N} w_{k,xy}^{(i)}w_{\ell,xy}^{(i)}\ A_i\right]$$

$$\beta_{k\ell}^{(6)} = Dv\left[\sum_{i=1}^{N} w_{k,xx}^{(i)}w_{\ell,yy}^{(i)}\ A_i\right]$$

$$\Gamma_{k\ell} = \Gamma_{k\ell}^{(1)} + \Gamma_{k\ell}^{(2)} + \Gamma_{k\ell}^{(3)}$$

where

$$\Gamma_{k\ell}^{(1)} = \frac{h}{2}\left[\sum_{i=1}^{N} \sigma_x w_{k,x}^{(i)} w_{\ell,x}^{(i)} A_i\right]$$

$$\Gamma_{k\ell}^{(2)} = \frac{h}{2}\left[\sum_{i=1}^{N} \sigma_y w_{k,y}^{(i)} w_{\ell,y}^{(i)} A_i\right]$$

$$\Gamma_{k\ell}^{(3)} = \frac{h}{2}\left[\sum_{i=1}^{N} \sigma_{xy} w_{k,x}^{(i)} w_{\ell,y}^{(i)} A_i\right]$$

When considering the fundamental, symmetric mode, $k = \ell = 1$, and $[\alpha]$, $[\beta]$ and $[\Gamma]$ reduce to first order matrices.

APPENDIX F

COEFFICIENT MATRICES FOR THE FUNDAMENTAL SYMMETRIC MODE

The numerical values of the coefficient matrices for the first symmetrical mode are given in this appendix. The matrices are given for four crack lengths. For each crack length the coarse and the refined stress distribution grids were considered. In the following, case I refers to coarse grid and case II refers to the refined grid for stress distribution.

a/(a+b)	Number of triangular elements	
	Coarse Grid, Case I	Refined Grid, Case II
0.4545	44	64
0.5681	44	78
0.6818	44	71
0.7954	57	89

a/(a+b)	α_{11}		β_{11}		Γ_{11}	
	Case I	Case II	Case I	Case II	Case I	Case II
0.4545	22.843307	22.869709	1081999.25	1099104.09	279275.65	280149.31
0.5681	21.263487	21.321285	894797.0	928155.04	273906.01	274890.21
0.6818	20.353329	20.436204	806567.06	818247.83	261905.35	270308.54
0.7954	19.923466	20.066635	743968.78	749917.88	269599.84	253750.88

APPENDIX G

COEFFICIENT MATRICES FOR THE COMBINATION OF FIRST TWO SYMMETRIC MODES

In this appendix second order coefficient matrices are presented. Again both the coarse and fine grids were used for each crack length. The number of elements for these grids were the same as used for one fundamental mode in Appendix F.

For $\frac{a}{a+b} = 0.4545$

(i) Coarse Grid

$$[\alpha] = \begin{bmatrix} 22.869709 & -.1746059 \\ -.1746059 & 10.679363 \end{bmatrix}, \quad [\beta] = \begin{bmatrix} 1081999.25 & 59754.61 \\ 59754.61 & 2427210.20 \end{bmatrix}$$

$$[\Gamma] = \begin{bmatrix} 279275.65 & -3384.96 \\ -3384.96 & 127393.51 \end{bmatrix}$$

(ii) Fine Grid

$$[\alpha] = \begin{bmatrix} 22.743396 & -.320774 \\ -.320774 & 10.479184 \end{bmatrix}, \quad [\beta] = \begin{bmatrix} 1099104.09 & 60285.95 \\ 60285.95 & 2381778.17 \end{bmatrix}$$

$$[\Gamma] = \begin{bmatrix} 280149.31 & -6590.07 \\ -6590.07 & 70804.46 \end{bmatrix}$$

For $\frac{a}{(a+b)} = 0.5681$

(i) Coarse Grid

$$[\alpha] = \begin{bmatrix} 21.263487 & -.119790 \\ -.119790 & 10.465988 \end{bmatrix}, \quad [\beta] = \begin{bmatrix} 874997.0 & +1130.75 \\ +1130.75 & 2343262.44 \end{bmatrix}$$

$$[\Gamma] = \begin{bmatrix} 273906.01 & -9884.79 \\ -9884.79 & 92312.99 \end{bmatrix}$$

(ii) Fine Grid

$$[\alpha] = \begin{bmatrix} 21.321285 & -.067658 \\ -.067658 & 10.616730 \end{bmatrix} \quad [\beta] = \begin{bmatrix} 928155.04 & 4681.08 \\ 4681.08 & 2343078.67 \end{bmatrix}$$

$$[\Gamma] = \begin{bmatrix} 274890.21 & -4076.62 \\ -4076.62 & 167500.62 \end{bmatrix}$$

For $\frac{a}{(a+b)} = 0.6818$

(i) Coarse Grid

$$[\alpha] = \begin{bmatrix} 20.353329 & .363351 \\ .363351 & 10.695647 \end{bmatrix}, \quad [\beta] = \begin{bmatrix} 786567.06 & 1777.22 \\ 1777.22 & 2290958.28 \end{bmatrix}$$

$$[\Gamma] = \begin{bmatrix} 261905.35 & -21525.3 \\ -21525.3 & 22867.74 \end{bmatrix}$$

(ii) Fine Grid

$$[\alpha] = \begin{bmatrix} 20.436204 & -.181150 \\ -.181150 & 10.862968 \end{bmatrix}, \quad [\beta] = \begin{bmatrix} 818247.83 & 6148.78 \\ 6148.78 & 2336680.46 \end{bmatrix}$$

$$[\Gamma] = \begin{bmatrix} 270308.54 & -13253.18 \\ -13253.18 & 124459.41 \end{bmatrix}$$

For $\frac{a}{a+b} = 0.7954$

(i) Coarse Grid

$$[\alpha] = \begin{bmatrix} 19.923466 & -1.085750 \\ -1.085750 & 9.774366 \end{bmatrix}, \quad [\beta] = \begin{bmatrix} 743968.78 & 12061.57 \\ 12061.57 & 2352239.72 \end{bmatrix}$$

$$[\Gamma] = \begin{bmatrix} 269599.84 & -86029.99 \\ -86029.99 & 233544.88 \end{bmatrix}$$

(ii) Fine Grid

$$[\alpha] = \begin{bmatrix} 20.066635 & -.144643 \\ -.144643 & 10.830553 \end{bmatrix}, \quad [\beta] = \begin{bmatrix} 749917.88 & 1530.41 \\ 1530.41 & 2352239.72 \end{bmatrix}$$

$$[\Gamma] = \begin{bmatrix} 253750.88 & 3438.31 \\ 3438.31 & 91725.86 \end{bmatrix}$$

REFERENCES

1. Baliaev, N. M., "Stability of Prismatic Rods Subjected to Variable Longitudinal Forces," Engineering Construction and Structural Mechanics, Leningrad, Russia, 1924, p. 149.

2. Einaudi, R., "About Unstable Equilibrium States of Plates Subjected to Periodic Shear Stresses," Atti. Accad. Gioenia, Memoria xx, 1935, p. 1.

3. Chelomei, V. N., "Dynamic Stability of Plates," Tr. Kiev. Aviats. Inst., No. 10, 1938.

4. Bodner, V. A., "Stability of Plates Subjected to Longitudinal Periodic Forces," Prikladnia Melematika, Vol. 2, No. 1, 1938, p. 87.

5. Bolotin, V. V., The Dynamic Stability of Elastic Systems, Holden Day, San Francisco, 1964.

6. Somerset, J. H. and Evan Iwanowski, R. M., "Influence of Non-Linear Inertia on the Parametric Response of Rectangular Plates," International Journal of Nonlinear Mechanics, Vol. 2, Sept. 1967, p. 217.

7. Willems, N. and Duffield, R. C., "Parametric Stability of Rectangular Plates Reinforced with Closely Spaced Stiffeners," Developments in Mechanics, Vol. 5, Iowa State University Press, 1969, p. 387.

8. Stahl, B. and Keer, L. M., "Vibration and Stability of Cracked Plates," International Journal of Solids and Structures, 1972, p. 69.

9. Lynn, P. P. and Kumbasar, N., "Free Vibration of Thin Rectangular Plates Having Narrow Cracks with Simply Supported Edges," Development in Mechanics, Vol. 4, p. 1967, p. 911.

10. Knowles, J. K. and Wang, N. M., "On the Bending of an Elastic Plate Containing a Crack," Journal Mathematical and Physics, 1960, p. 223,39.

11. Hartranft, R. J. and Sih, G. C., "Effect of Plate Thickness on the Bending Stress Distribution Around Through Cracks," Journal Mathematical Physics, 47, 1968, p. 276.

12. Lukaart, C. A., "Vibration of Cracked Plates," Ph.D. Thesis, Georgia Institute of Technology, Jan. 1975.

13. Petyt, M., "The Vibration Characteristics of a Tensioned Plate Containing a Fatigue Crack," Journal of Sound and Vibration," 1968 8 (3), 377-389.

14. Backer, G. C., "Static and Dynamic Behavior of Tensioned Doubly Connected Plates," Ph.D. Thesis, Georgia Institute of Technology, August, 1972.

15. Datta, P. K., "On the Buckling and Vibration Behavior of a Thin Tensioned Sheet with an Elliptical Hole," Ph.D. Thesis, Georgia Institute of Technology, June 1972.

16. Carlson, R. L., "An Experimental Study of the Parametric Excitation of a Tensioned Sheet with a Cracklike Opening," Experimental Mechanics, November 1974.

17. Timoshenko, S. P. and Woinowsky-Krieger, S., Theory of Plates and Shells, McGraw Hill Book Company, 1959, Second Edition.

18. Marguerre, K., "Zur Theorie der gekrummten Platte grosser Formanderung," Proc. 5th Intern. Congr. Appl. Mechanics, pp. 93-101, Cambridge, Mass. 1938.

19. Hildebrand, F. B., Methods of Applied Mathematics, Prentice Hall, Englewood Cliffs, N. J., 1952.

20. Meirovitch, L., Analytical Methods in Vibration, The McMillan Co., 1969.

21. Aberson, J. A. and Anderson, J. M., "Cracked Finite Elements Proposed for NASTRAN," 3rd Annual NASTRAN User's Colloquim, NASA Langley Research Center, September 1973.

22. Riggs, D., "Experimental Investigation on Buckling of Thin Plates in Tension," Special Project, Aerospace Engineering, Georgia Institute of Technology, Spring 1974.

23. Warburton, G. B., "The Vibration of Rectangular Plates," Proc. of the Institute of Mechanical Engineers, Vol. 168, 1954, p. 371

24. Datta, P. K. and Carlson, R. L., "Buckling and Vibration of a Thin Tensioned Sheet with an Elliptical Hole," Experimental Mechanics, Vol. 13, No. 9, pp. 280-289, July 1973.

25. Zielsdorf, G. F. and Carlson, R. L., "On the Buckling of Thin Tensioned Sheets with Cracks and Slots," Presented at the Symposium on Fracture and Fatigue, George Washington University, May 3-5, 1972.

26. Williams, M. L., "On the Stress Distribution at the Base of a Stationary Crack," Journal of Applied Mechanics, Vol. 24, March 1957, pp. 109-114.

27. Zienkiewicz, O. C., The Finite Element Method in Engineering Science, McGraw Hill, London, 1971.

28. Przemieniecki, J. S., Theory of Matrix Structural Analysis, McGraw Hill Inc., 1968.

29. ICES-STRUDL-II, Vol. 2, Department of Civil Engineering, MIT, Second Edition, June 1971.

30. Gross, B., Srawley, J. and Brown, W. F., "Stress Intensity Factors for a Single-Edge-Notch Tension Specimen by Boundary Collocation of a Stress Function," NASA Technical Note, NASA IN D-2395, August 1964.

31. Williams, M. L., "The Bending Stress Distribution at the Base of a Stationary Crack," Journal of Applied Mechanics, Vol. 28, No. 1, March 1961, pp. 78-82

32. ICES-STRUDL-II, Vol. 1, Department of Civil Engineering, MIT, First Edition, Nov. 1968.

VITA

Som P. S. Virk was born on May 15, 1949 in Jamshedpur, India. He graduated from Government High School, Phagwara (India) in 1965, and obtained his B. Sc. in Aeronautical Engineering from Panjab University in 1971. He entered Georgia Institute of Technology in the Fall, 1971, earned his M.S. in December 1972, and continued as a research assistant in the School of Aerospace Engineering.